Rev. Date: 2/24/2014

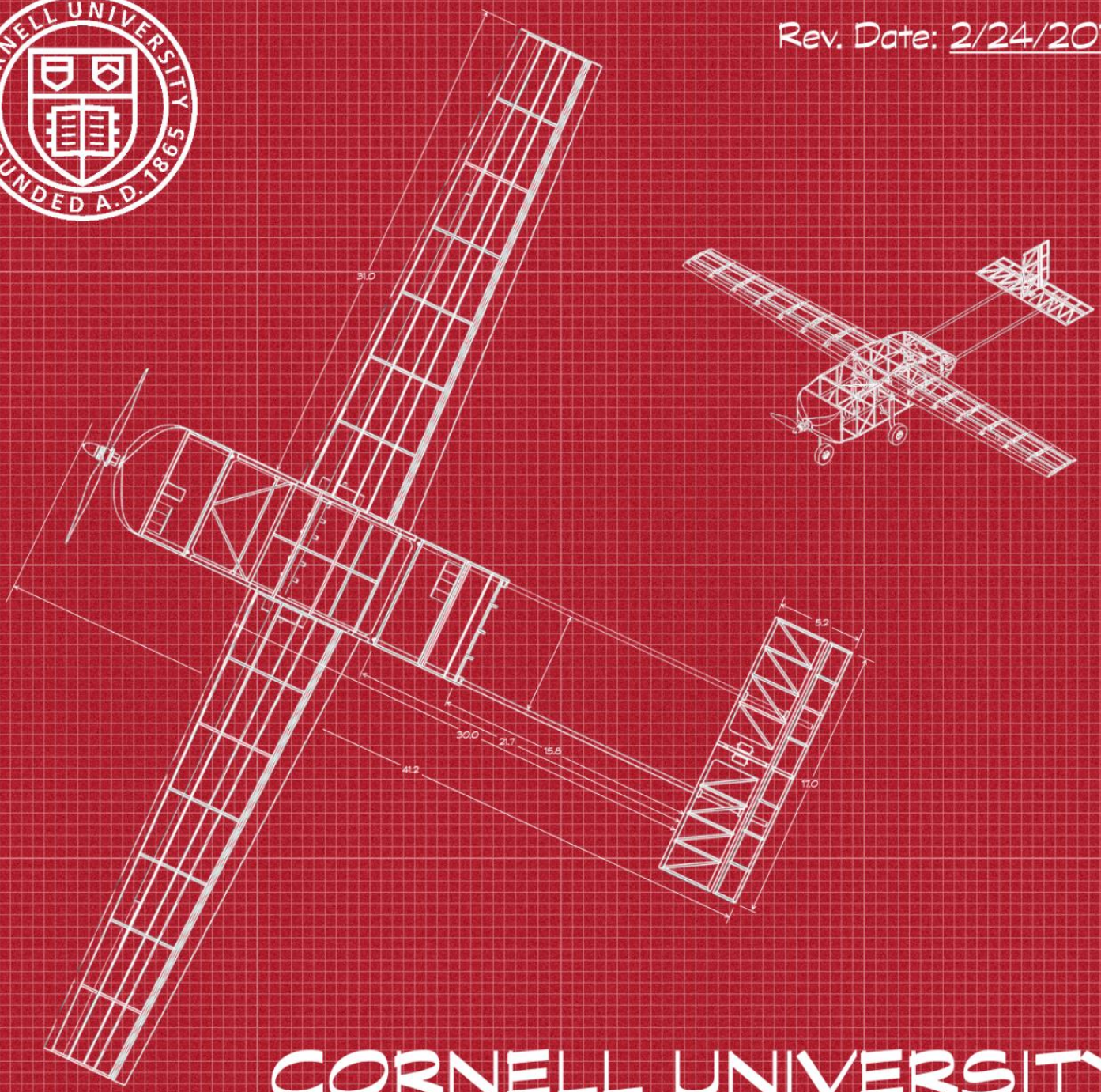

CORNELL UNIVERSITY

2013-2014 Aircraft Design Report

Cessna/Raytheon/AIAA Design-Build-Fly Competition

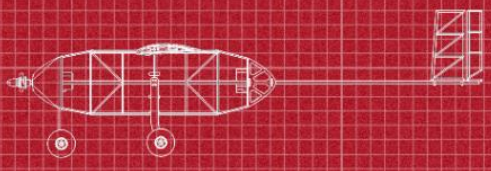

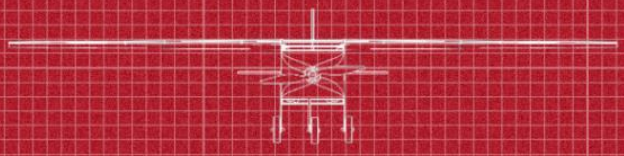

1 Executive Summary

The following report details the design, analysis, manufacturing, and testing conducted by Cornell University's Design Build Fly project team during 2013-2014 competition year. The goal of this team is simple: produce a custom radio-controlled aircraft that will win the 2013-2014 AIAA/Cessna/Raytheon Design/Build/Fly competition. The team attempted to accomplish this by creating an aircraft design that meets all of the competition constraints, performs well in all four of the competition missions, and minimizes the aircraft's weight. The first mission of the competition is a taxi mission, requiring the aircraft to navigate a course of rough terrain without becoming airborne. All subsequent missions are flight missions: one empty and two carrying internal payloads. The payloads consist of wooden blocks of various shapes and weights, some of which must be carried in specific orientations. The craft must also take off within a 40 foot runway.

A careful analysis of the competition scoring showed the most important scoring parameter of the aircraft to be weight, followed by speed, and the quantity of payloads carried. These requirements and scoring analysis were used to generate a design consisting of a conventional configuration with minimized weight, a single tractor motor, tricycle landing gear, a conventional tail, and a capacity of two payloads for mission two. These attributes were all chosen with the direct intention of increasing overall competition score.

After reaching a conceptual design, the team was split into four subteams: aerodynamics, stability/controls, structures/integration, and propulsion. Each of these subteams performed detailed design, analysis, and testing to optimize their respective subsystems for a maximum overall competition score.

Finally, the team constructed several prototypes of our design in order to validate our analysis and expected performance. This process uncovered a number of unforeseen problems and areas for improvement. Iteration of the design and analysis process will continue to improve the performance of the aircraft up until competition. Figure 1 shows our estimated scoring for our final aircraft design. Our team is very excited to participate in our third Design/Build/Fly competition.

Mission 1		**Mission 2**		**Mission 3**	
Laps flown.	7	Payload Flown	2	3 lap time (s)	112
Estimated max.	8	Estimated max.	5	Estimated min.	100
Empty Weight (lb)		**Taxi Score**		**FLY-OFF SCORE**	
2.056		1.0		**4.23**	

Figure 1 – Scoring estimates for final aircraft design (report score not included)

2 Management Summary

The Cornell Design Build Fly team consists of 20 undergraduate and graduate students with a shared passion for aeronautics and aircraft design. The team spent the first several weeks studying the competition rules and requirements, conducting scoring analysis and trade studies to identify driving design requirements, and developing a conceptual design. The team then divided into subteams for the preliminary design, detailed design, fabrication, and testing phases of the project.

2.1 Team Organization

The technical portion of the project was completed by a group of four subteams, each responsible for their respective subsystems: aerodynamics, stability/controls, structures/integration, and propulsion. Figure 2.1 depicts the organization of the team. Team members were assigned to a subteam based on their interest and past experience. Subteam leaders keep their team on schedule, facilitate communication with other subteams, and mentor less experienced members of their subteam.

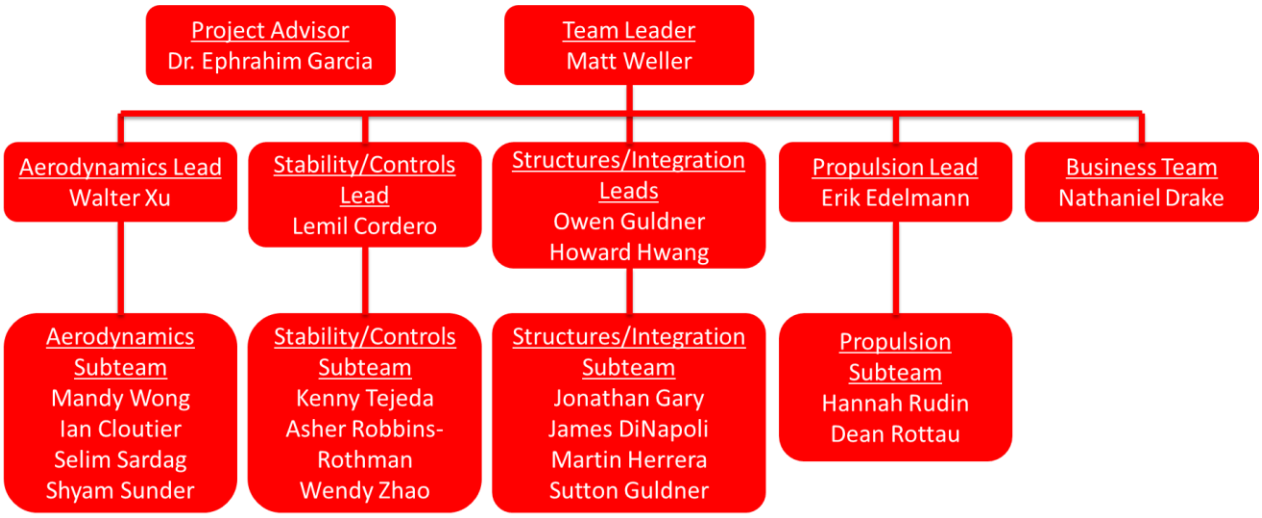

Figure 2.1 – Team Structure

2.2 Milestone Chart

Our team utilized a milestone chart throughout the course of this project in order to ensure that key design tasks were completed in a timely fashion. The chart, shown in figure 2.2, displays planned and actual timing of the key elements of the design process.

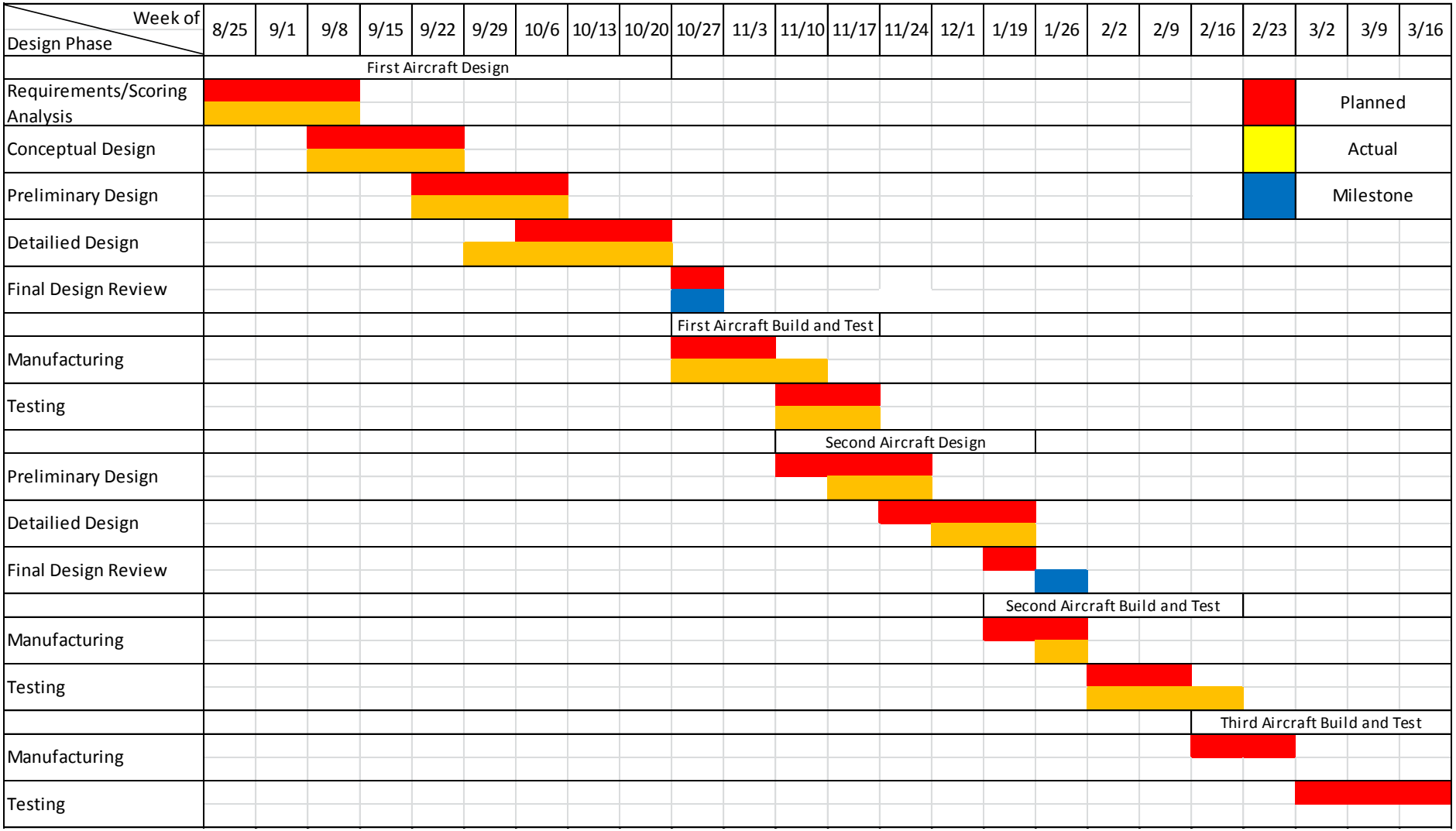

Figure 2.2 – 2013-2014 Cornell DBF Milestone Chart

3 Conceptual Design

During the conceptual design phase of the project, the team closely examined the 2014 mission profile and scoring function. We then performed an in depth scoring analysis and researched the advantages of differing aircraft configurations with respect to this year's scoring.

3.1 Mission Requirements and Scoring

The 2014 AIAA DBF competition is comprised of one taxi mission and three independent flight missions. A maximum score will be obtained by successfully completing all missions, while complying with all mandated constraints and optimizing weight, speed, and payload capacity of the aircraft.

3.1.1 General requirements

Several requirements hold for all flight missions. The aircraft must complete a rolling take-off within a forty foot long runway. It must also land on the runway without sustaining any significant damage. All payloads must be loaded into the aircraft in a five minute period prior to a mission attempt. The same course must be flown for each flight mission, as shown in Figure 3.1.1.

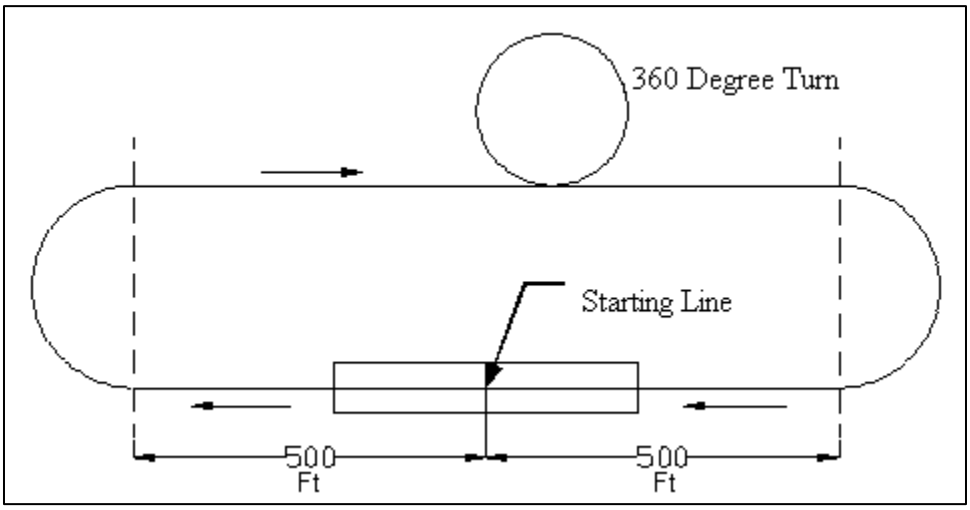

Figure 3.1.1 – Flight course layout

A number of general constraints also apply to the propulsion system. Electric motors must be used and battery chemistry is limited to either NiMH (Nickel-Metal-Hydride) or NiCd (Nickel-Cadmium). The propulsion batteries must not exceed 1.5 pounds, and the current in any propulsion component must not exceed 15 amps.

3.1.2 Scoring summary

The teams score will be determined by the following formula:

$$SCORE = Written\ Report\ Score * \frac{Taxi\ Score * Flight\ Score}{Empty\ Weight}$$

The report is scored out of a maximum of 100 by judges. The flight score is the sum of the individual flight mission scores. These scores and the taxi score are detailed in the mission descriptions below. Empty weight is the maximum weight of the aircraft without payloads, and is measured in pounds after each successful mission.

3.1.3 Taxi mission – rough field taxi

The objective of the Taxi mission is to traverse a 40 by 8 foot course of rough terrain. The terrain is constructed of corrugated fiberglass roofing material with 0.625" ridges spaced 3" apart. Standard 2x4's on their edge act as obstacles (3.5" tall), extending across half of the course width and placed at 1/3 and 2/3 of the length of the course as shown in Figure 3.1.3. The aircraft must have adequate ground clearance for one of these standard 2x4's to be passed under the wing anywhere beyond ¼ wingspan from the aircraft centerline.

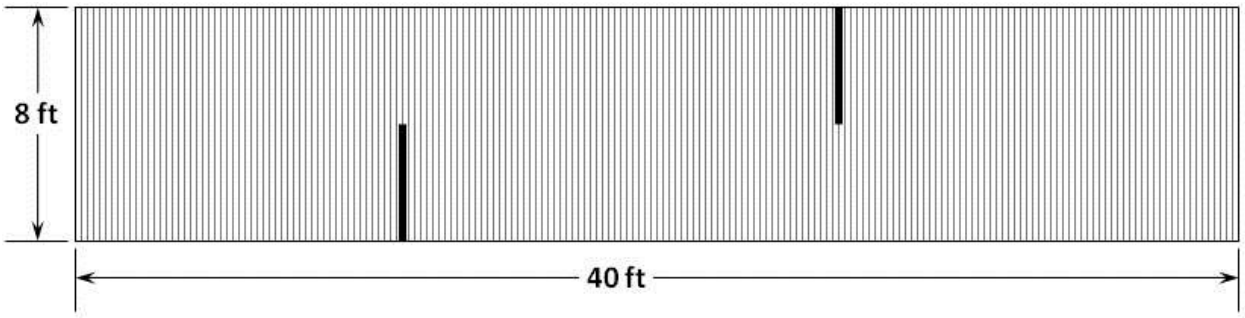

Figure 3.1.3 – Taxi Mission Course Layout

The payload from flight mission 3, described below, must be carried during the taxi mission. The aircraft must complete the course within five minutes without leaving the sides of the course or becoming airborne. The craft must not sustain any damage during the completion of this mission. The taxi score will be 1 if successful or 0.2 if unsuccessful.

3.1.4 Mission 1 – ferry flight

The objective of this mission is to complete as many laps around the flight course as possible within a 4-minute flight time. The timer starts when throttle is advanced for take-off and ends after four minutes. A lap is completed when the aircraft crosses the start line and only complete laps are counted for scoring. The performance in this mission is normalized across all teams successfully completing the mission by the following formula:

$$M1\ Score = 2\ x\ \frac{Number\ of\ laps\ flown\ by\ team}{Maximum\ number\ of\ laps\ flown\ in\ competition}$$

3.1.5 Mission 2 – maximum load mission

This mission requires the aircraft to complete three laps around the course with an internal payload of simulated cargo boxes. The cargo boxes are 6" x 6" x 6" wooden cubes and are ballasted to 1

pound each. Scoring for this mission is determined by the number of payloads carried according to this formula:

$$M2\ Score = 4\ x\ \frac{Number\ of\ payloads\ carried\ by\ team}{Maximum\ number\ of\ payloads\ carried\ in\ competition}$$

3.1.6 Mission 3 – emergency medical mission

This mission is designed to simulate the transport of two patient gurneys and two attendants in an emergency situation. Patient gurneys will be simulated by 9" x 4" x 2" wooden blocks, ballasted to 0.5 pounds each. Attendants will be simulated by 6" x 2" x 4" blocks, also ballasted to 0.5 pounds each. The attendant must be oriented vertically and the patient must be horizontal and flat as shown in Figure 3.1.6. The attendant must be immediately adjacent to the side of the patient. Additionally, at least two inches of space above the patients must be free of any structure or systems. Patients must be separated by a minimum of two inches side to side, or above/below, and attendants must be at least two inches from each other.

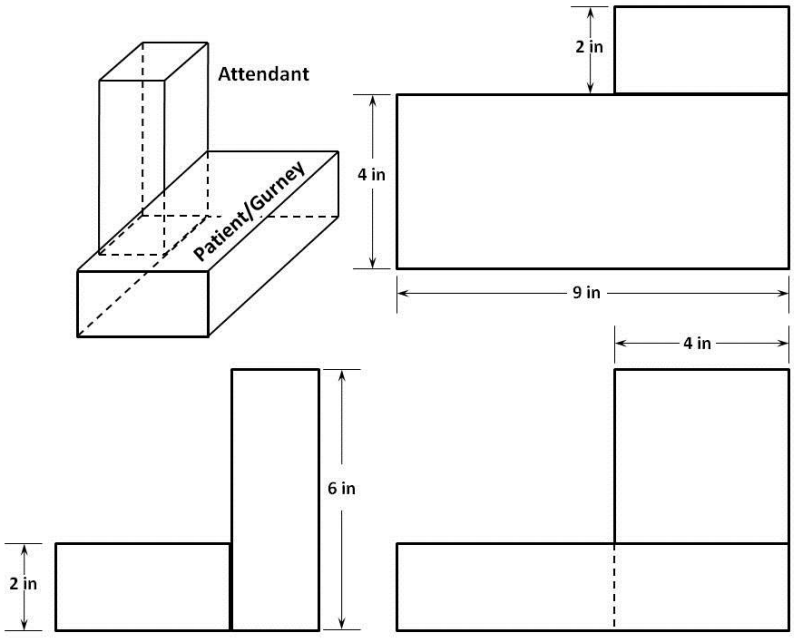

Figure 3.1.6 – Mission three payload arrangement specifications.

The aircraft must complete three laps of the course with two attendant/patient combinations carried internally. The scoring timer begins when throttle is advanced for take-off and stops when the start/finish line is crossed at the end of the third lap. The scoring of this mission is based on speed and is found through this formula:

$$M3\ Score = 6\ x\ \frac{Fastest\ time\ flown\ in\ competition}{Team\ time\ flown}$$

3.2 Design Requirements

In order to better understand the effects of aircraft design parameters on the overall competition score, our team conducted an in-depth scoring analysis. We determined empty weight, cruise velocity, and M2 payload quantity to be the design variables that directly affect our score. While the taxi mission also affects the overall score, its effect is so drastic that we determined the mission to be essential in generating a competitive score. With this in mind, we chose to treat completion of the taxi mission as a constraint and not a design variable. Based on research of past competitions with similar design constraints, we were able to develop estimated values for mean and standard deviation of each of the design variables. By combining those values with this year's scoring function, we were able to simulate the overall scoring effects of perturbations to each of the design variables. This simulation was conducted using MATLAB and its results are shown in Figure 3.2a. Each line in the plot depicts how our overall score would change by varying the parameter it represents while holding all others constant.

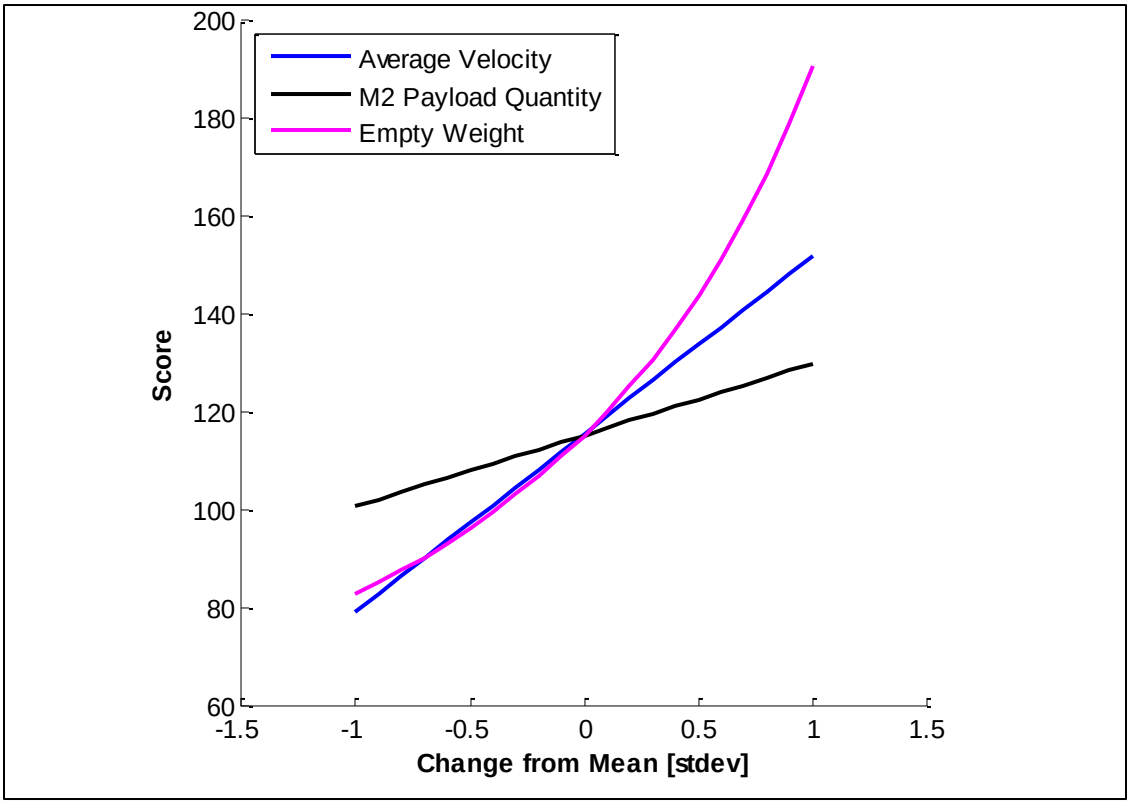

Figure 3.2a – MATLAB scoring analysis

Using the output of this scoring analysis we were able to prioritize the optimization parameters of our design to favor weight reduction, followed by speed increase, and finally, increased payload capacity. Based on this prioritization we were able to complete a translation of competition requirements into key design requirements for our aircraft. The most important design requirements are driven by mandated competition constraints, since failure to complete them will preclude any measure of success in the competition. To meet these constraints the aircraft must have enough lift and static thrust to take-off

within 40 feet while carrying at least 2lbs of payload. The aircraft must fly in a stable and controlled manner to ensure course completion and safe landings. Our design must also be stable, controllable, and robust enough to successfully complete the rough terrain taxi mission. While ensuring that these constraints are met, our team strove to optimize our score by prioritizing the design variables as described above: 1) Weight reduction, 2) Speed increase, 3) Payload capacity increase.

Competition Requirement	Design Requirement
Complete all missions with the lightest possible aircraft.	Minimize the weight of all systems
Complete rough terrain taxi mission	Adequate ground handling and maneuverability on rough terrain
Accommodate all Payloads	Aircraft must lift at least 2lb of payload
Take-off within 40ft runway	Adequate wing area and static thrust
Take off and land successfully for all missions	Adequate static and dynamic stability

Figure 3.2b – Translation of competition requirements into key design requirements

3.3 Concept Selection Process

In order to generate as many potential concepts as possible, the team completed initial brainstorming as an individual exercise. Each member drew upon intuition and past experience to develop ideas that would effectively meet the requirements. This was then followed by a group brainstorming session in which each member presented their ideas to the entire team. Through this process, each member of the team was able to provide feedback and further develop all of the proposed ideas.

After completion of the brainstorming process, the team used decision matrices to objectively evaluate each of the generated concepts. The categories in which concepts were evaluated were: wing configuration, motor configuration, landing gear configuration, and tail configuration. For each system, the team compared configurations by rating them based on parameters deemed critical to the success of the given system. The team then weighted the parameters for each decision matrix based on importance. The parameter weights in this matrix are primarily derived from the initial design goals, placing higher weights on components that were deemed more important in the scoring analysis and mission constraints. This selection process enabled us to select the configurations that would maximize the aircraft's score at competition.

3.3.1 Wing configuration

Weight, lift to drag ratio, and stability were the primary categories considered in the selection of a wing configuration, along with secondary categories of integration, manufacturability, and ground clearance. The importance weights are derived from our analysis of scoring parameters and mission constraints. Based on these categories, a high-wing configuration scored significantly higher than others.

Metric	Importance	High wing	Low Wing	Mid wing	Bi-Plane	Flying Wing
Weight	0.3	4	4	4	3	4
L/D	0.25	3	3	3	3	4
Stability	0.25	5	2	4	3	2
Integration	0.1	4	4	5	3	2
Manufacturability	0.05	3	3	3	2	2
Ground Clearance	0.05	4	2	4	5	2
Total		**3.95**	**3.1**	**3.8**	**3.05**	**3.1**

Figure 3.3.1 – Wing Configuration Decision Matrix

3.3.2 Motor configuration

Areas of concern during the selection of a motor configuration included thrust to weight ratio, structural integration, stability, and ground maneuverability. As a result of this analysis the team determined that a single tractor configuration would best meet the requirements of the competition.

Metric	Importance	Single Pusher	Single Tractor	Double Pusher	Double Tractor	Tandem
Thrust to Weight	0.4	3	3	2	2	2
Integration	0.3	2	3	2	2	2
Stability	0.2	2	4	2	4	3
Ground Maneuverability	0.1	2	2	4	4	2
Total		**2.4**	**3.1**	**2.2**	**2.6**	**2.2**

Figure 3.3.2 – Motor Configuration Decision Matrix

3.3.3 Landing gear configuration

Selection of a landing gear configuration took several factors into consideration based on our scoring analysis and mission requirements. These categories included weight, drag, shock absorption, ground controllability, and integration. A tricycle configuration scored best due to its relatively good shock absorption and controllability as well as average scores in all other categories.

Metric	Importance	Tricycle	Tail Dragger	Wheels on Skids
Weight	0.35	3	3	4
Drag	0.25	3	3	4
Shock Absorption	0.2	4	4	1
Controllability	0.15	4	3	3
Integration	0.05	3	3	3
Total		**3.35**	**3.2**	**3.2**

Figure 3.3.3 – Landing Gear Configuration Decision Matrix

3.3.4 Tail configuration

A tail configuration was chosen based on the performance parameters of stability, weight, integration, drag, and manufacturability. The conventional tail design scored best due to good marks in all areas and exceptional stability performance.

Metric	Importance	Conventional	V-tail	Canard	Twin-Tail	T-Tail
Stability	0.4	5	4	2	5	4
Weight	0.2	3	4	3	3	2
Integration	0.2	3	2	2	2	3
Drag	0.1	3	3	4	3	4
Manufacturability	0.1	4	3	3	4	3
Total		**3.9**	**3.4**	**2.5**	**3.7**	**3.3**

Figure 3.3.4 – Tail Configuration Decision Matrix

3.4 Selected Concept

Figure 3.4 shows the results of the conceptual design phase. The design combines the results of the decision matrices into a comprehensive design. The conventional design minimizes weight while providing a structurally robust and aerodynamically stable platform. Structural components are centralized around the wing, landing gear, and payload compartment to minimize weight. The remainder of the lightweight fuselage is strictly for enclosing the payloads. A tricycle landing gear provides stability during the taxi mission. The concept is designed to be as lightweight as possible while still adequately completing all mission objectives.

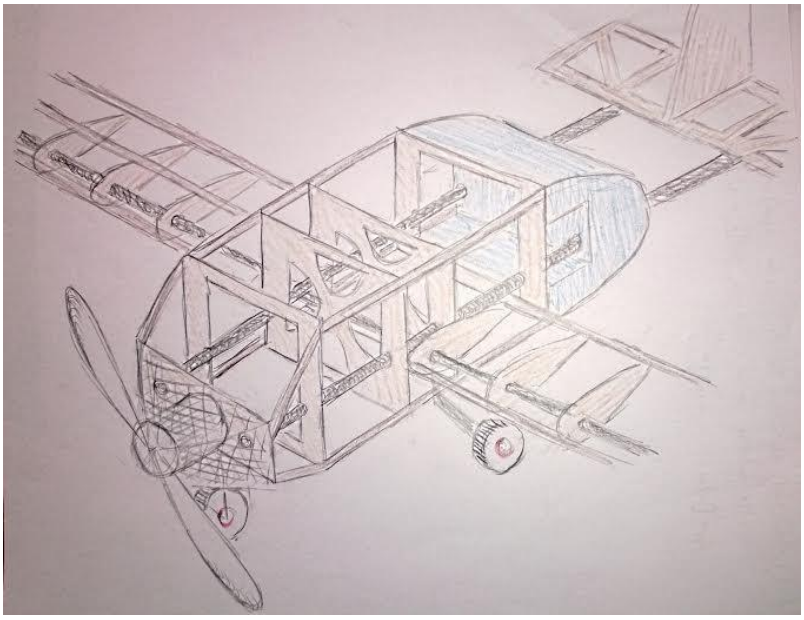

Figure 3.4 – Conceptual Design sketch

4 Preliminary Design

During the preliminary design phase, the team used the results of conceptual design to determine sizing and performance parameters of the aircraft's major systems. Through design iteration, we optimized the aircraft to best meet our critical design requirements.

4.1 Design and Analysis Methodology

Aircraft design and analysis is an inherently circular process; the characteristics of various subsystems are largely dependent upon each other. Due to this, our team relied on an iterative development process in order to maximize our aircraft's potential score at competition. The design wheel in Figure 4.1a depicts the methodology utilized by our team. Initially, design requirements developed during conceptual design drove the characteristics of the first design concept. Some of these requirements needed further investigation in the form of sizing and trade studies. Upon completion of an initial design concept, analysis raised new questions and opportunities for improvements. This led to further trade studies, requirements, and ultimately a new design concept.

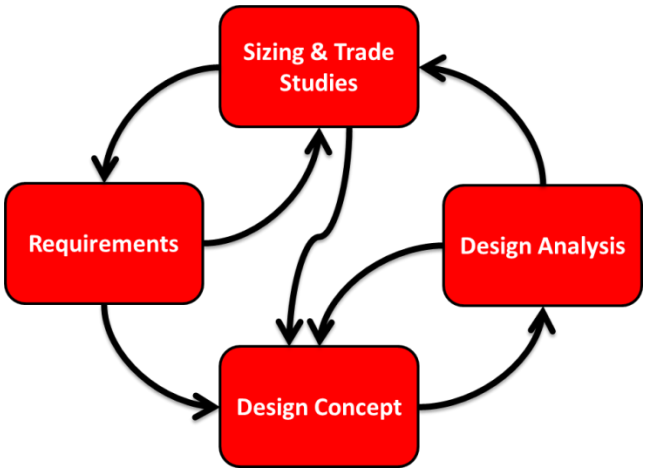

Figure 4.1a – The Design Wheel

The preliminary design phase begins with the overarching design requirements and concept developed during the conceptual design phase. Figure 4.1b illustrates the conceptual and preliminary design phases. Initial sizing and trade studies develop the conceptual design into a preliminary design. At this point weight distribution is estimated and stability is ensured. These parameters then drive the required performance of the aerodynamic and propulsion systems. Finally, a full system performance analysis yields opportunities for improvement and a new preliminary design is generated. This process is continued until an optimal design is reached.

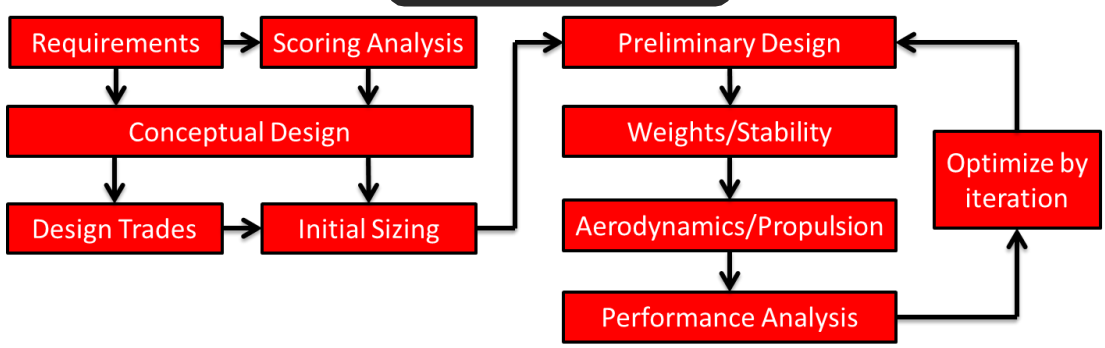

Figure 4.1b – Design Process Diagram

4.2 Design and Sizing Trades

Our team employed a single design and sizing trade study at the full aircraft level to make an informed decision about the number of payloads that should be carried for mission two. This study allowed us to examine the effect of payload quantity on our overall competition score. Any subsystem level trade studies are covered in their respective preliminary design section.

Due to its influence on many of the aircraft's systems, the quantity of payloads to be carried for mission two was determined early in the preliminary design process. This was accomplished by calculating flight scores across a wide range of potential aircraft configurations which varied in the number of payload carried, as well as speed, maximum number of payloads carried at the competition, and payload factor (payload weight/gross weight). A reduced set of data is shown in Figure 4.2. While similar results were seen with all combinations of input parameters, this example assumes that we are the fastest aircraft at competition and the maximum number of stores carried by any team is five. This study revealed that the score benefit of adding a payload is overshadowed by the corresponding weight penalty. The drop in score when carrying one payload is explained by mission three's requirement to carry two pounds of payload. Based on these results the team made the decision to carry two cargo box payloads for mission two.

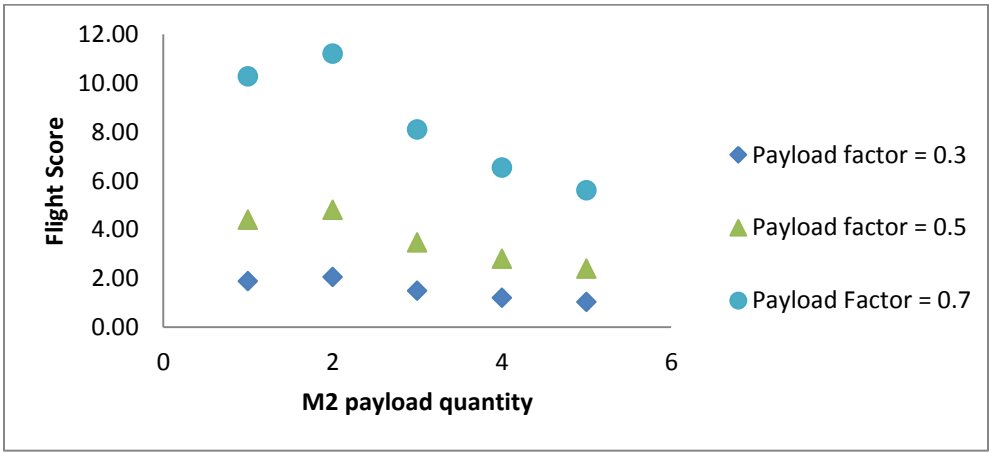

Figure 4.2 – Effect of payload quantity on flight score

4.3 Mission Model – Capabilities and Uncertainties

The team utilizes a custom mission model developed using MATLAB programming software with the primary goal of optimizing aircraft systems to best meet competition requirements. The program facilitated the sizing of aircraft components, performance estimates, and flight score calculations based on inputted aircraft parameters and a model of the aircraft's flight trajectory. The flight course is simulated using four discrete flight phases: takeoff, climb, cruise, and turn, as shown in figure 4.3a.

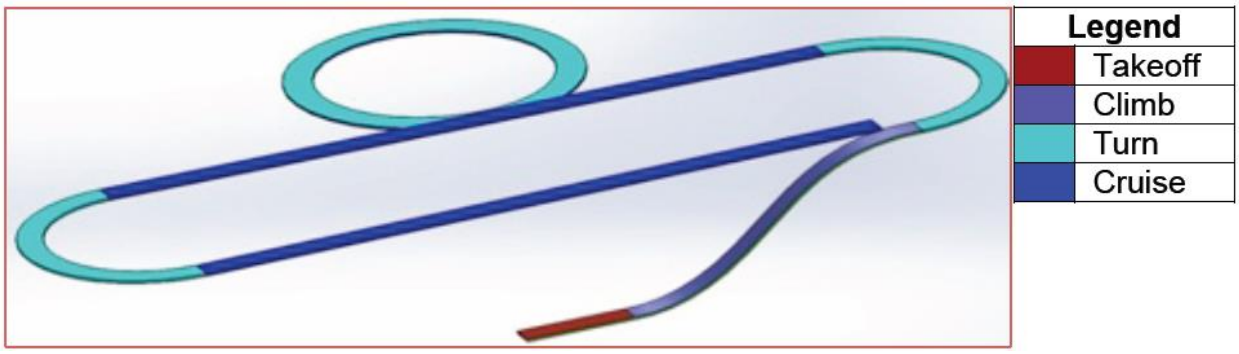

Figure 4.3a – Flight course simulated in mission model

Each flight phase has unique constraints governing its equations of motion in the mission model, as summarized in Figure 4.3b. The model shown is used for missions one through three. The mission model also accounts for accelerated flight between the climb and cruise phases of the flight course, as well as following the turn phases of flight. We used a turn load factor of five for mission one, and three for missions two and three to estimate the additional lift required during turns.

Flight Phase	Description	Constraints Modeled
Takeoff	Acceleration from standstill until lift equals weight	AoA = constant
Climb	Climb from ground to safe flight attitude	AoA = constant
Cruise	Level, unaccelerated flight at optimal angle of attack	L = W, T = D
Turn	Sustained, constant speed, level turns at maximum allowable load factors (different for each mission)	L = nW, T = D
AoA = angle of attack, L = lift, W = weight, T = thrust, D = drag, n = load factor		

Figure 4.3b – Summary of flight phases simulated in mission model

The mission model presented here possesses several uncertainties that limit the scope of its accuracy. Since all inputs to the model are only estimates and not representative of actual aircraft performance, the outputs obtained from the program are only estimates as well. The model does not account for wind conditions during flight; doing so adds significant variability to performance estimates. Battery voltage is treated as constant and equal to the nominal cell value throughout flight. Finally, the model neglects ground rolling friction, interference drag, and compressibility effects. In order to account for these uncertainties, we use the model as a tool in conjunction with extensive testing, which ensures that we ultimately attain the best results.

4.4 Propulsion Characteristics

The propulsion subteam was responsible for selecting all of the electronic components necessary for powering the aircraft. This consisted of first developing a system for ranking complete propulsion systems and then selecting and optimizing a system to maximize flight score while meeting all competition constraints.

4.4.1 Propulsion figure of merit

In order to quantitatively rank propulsion systems, the propulsion subteam developed a figure of merit relating the competition scoring to aspects of the design directly influenced by the propulsion system. The figure of merit serves as our descriptive metric for comparing propulsion systems.

Before being multiplied by the written report score, the total score an aircraft receives at the competition is dependent on the Total Mission Score divided by the Empty Weight of the aircraft.

$$Score = \frac{Total\ Mission\ Score}{Empty\ Weight}$$

The Total Mission Score is the product of the Taxi Score and the Flight Score (the sum of the three flight missions, M1 + M2 + M3). Mission 1 score is dependent on the speed of the airplane. Mission 2 is solely scored based on the number of payloads the aircraft can successfully carry. Mission 3 is also dependent on the speed of the airplane.

$$Flight\ Score = M1 + M2 + M3 = 2 * [speed] + 4 * [payloads] + 6 * [speed]$$

Assuming successful completion of the Taxi Mission, the total score can be approximated as a function of the speed of the airplane divided by its weight:

$$Score \approx f\left(\frac{speed}{empty\ weight}\right)$$

The propulsion system contributes directly to the empty weight of the airplane, and also influences thrust. In order for an airplane to travel at a constant velocity, the thrust must be equal to the drag force. Therefore the thrust generated by the propulsion system must be directly proportional to the drag force on the aircraft.

$$Thrust \propto Drag$$

The equation for drag force is $F_D = \frac{1}{2}\rho A C_D v^2$; therefore:

$$Thrust \propto Drag \propto Speed^2 \rightarrow Speed \propto \sqrt{Thrust}$$

Finally, the metric is complete, based entirely on aspects of the score directly influenced by the propulsion system.

$$Score \propto \frac{\sqrt{Thrust}}{Weight}$$

Based on this figure of merit, weight reduction became the primary factor in evaluating propulsion systems. The final propulsion system was chosen from those that had the greatest figure of merit.

4.4.2 System requirements/constraints

While this figure of merit is useful for evaluating propulsion systems, it is unable to distinguish between systems of different scales. A few constraints on the selection process greatly improved the usefulness of the figure of merit.

The first limitation was the motor current draw. Competition rules mandate that a 15 amp fuse limit this value, so we only considered configurations that were in adherence. This value largely dictated which motor, gear ratio, and propeller we used. Larger gear ratios and propellers tend to maximize static thrust and minimize current draw. This focused our search for an optimal motor.

The second limitation was the approximate minimal thrust required for takeoff within 40ft. In order to approximate this value, we made a series of assumptions. First, we assumed a takeoff speed of 30ft/s. This was purely from historical precedence, and matches well with many RC airplanes of this scale. The second assumption was that thrust is constant during takeoff. This assumption is later validated in section 4.4.4. We also assume negligible rolling friction. A constant drag force of 3N was estimated based on calculations from the aerodynamics subteam. Lastly, a 4.5lbs gross takeoff weight was deemed appropriate based on payload requirements and empty weight goals. The following set of equations was then developed.

$$V_f{}^2 - V_o{}^2 = 2ad \qquad a = \frac{F}{m} \qquad F = \frac{V_f{}^2 m}{2d} = 2.25lbf$$

Based on the large number of assumptions being made and the importance of meeting the takeoff distance requirement, we decided to add an additional 50% safety margin, bringing our goal for minimum static thrust to 3.375lbf.

4.4.3 Component selection:

With the assistance of a trusted online propulsion system calculator (www.ecalc.ch), the team completed the iteration process shown in figure 4.4.3a on more than 100 potential propulsion systems.

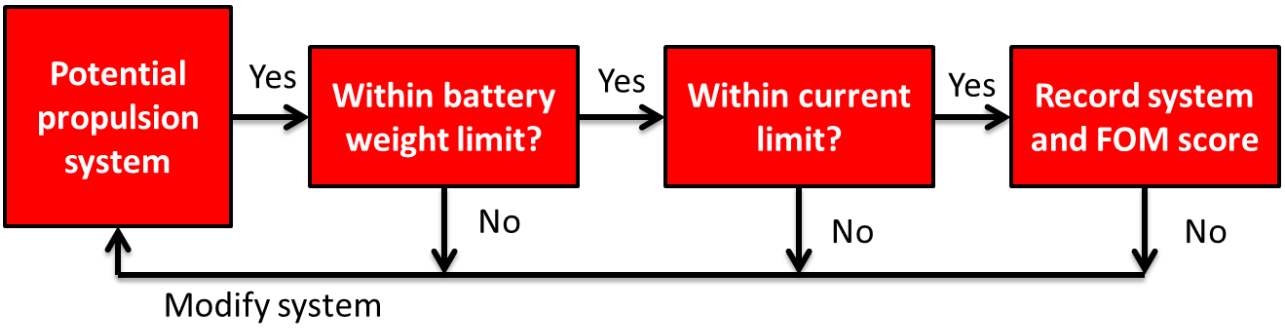

Figure 4.4.3a – Propulsion system iteration process

The team was then able to establish a list of high-scoring systems. This group of systems is depicted in Figure 4.4.3b. Using this tool, we were able to select the propulsion system that exhibits the best figure or merit while still meeting our minimum requirements.

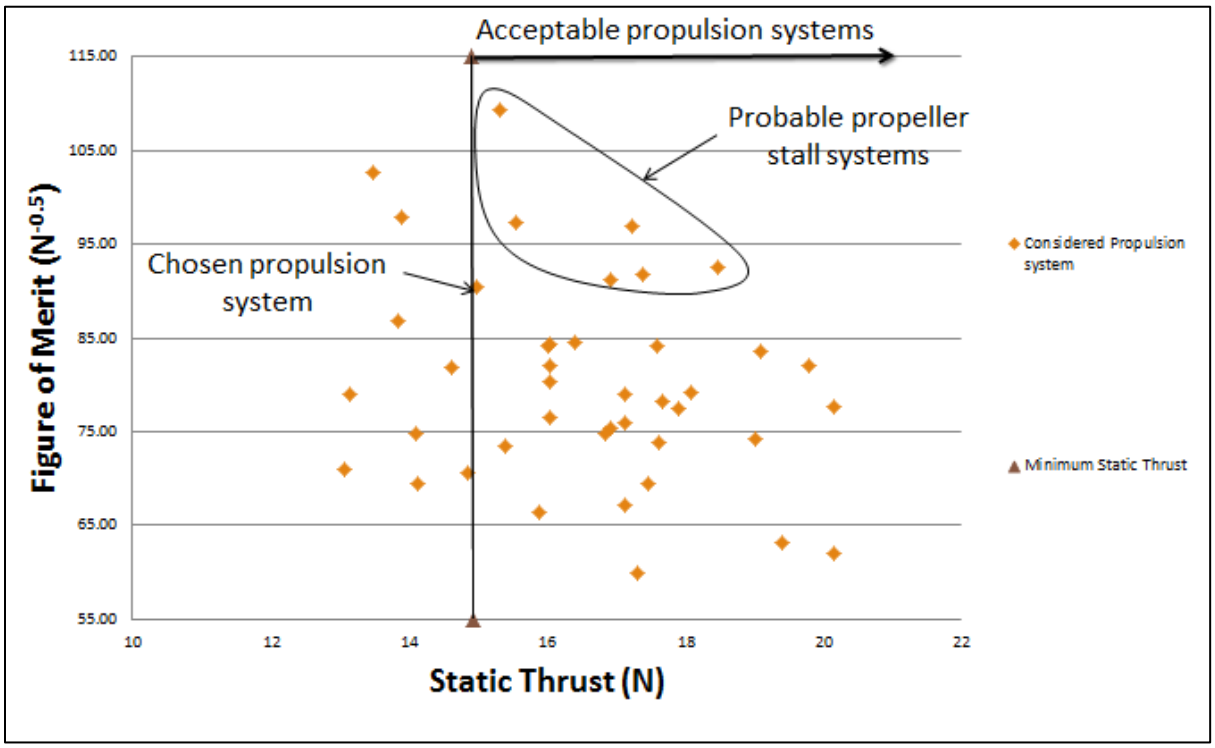

Figure 4.4.3b: Short list of acceptable propulsion systems

The propulsion system chosen through this method employs the components in figure 4.4.3c. Since mission one is an empty flight, it has reduced static thrust needs. This enables us to use a higher pitch-to-diameter ratio to bias the optimal performance point to higher airspeeds.

Component	Details
Battery	13x Elite 1500 NimH
Motor	Neu Motors 1105/6D
Gear Drive	Neu Motors P29 6.7:1
Propeller	APC 13x8 (Mission 2&3) APC 12x10 (Mission 1)

Figure 4.4.3c – Propulsion system selected components

4.4.4 Propeller optimization

We plan to take full advantage of propeller interchangeability between missions at the competition. In order to confirm the accuracy of our eCalc results, we utilized our own mission model's propulsion system calculation tools. Figure 4.4.4a shows the thrust, power, current draw, and RPM for each propeller we intend to use with this system.

Propeller	Thrust (lbf)	Power (lbf.ft/s)	Current draw (amps)	RPM
APC 12x10 E	2.87	159	14.7	36,900
APC 13x8 E	3.30	175	16.9	35,200

Figure 4.4.4a – Mission model propulsion simulation

Figure 4.4.4b depicts the thrust generated by the 12x10 propeller and current drawn from the batteries as a function of airspeed. Figure 4.4.4c plots the power required to sustain lift for each mission, as well as the power available from the propulsion system as a function of airspeed. M2 and M3 are overlaid due to nearly identical mission conditions. This graph provides insight into a potential top speed of 77 ft/s based on the intersection of the needed and available power curves.

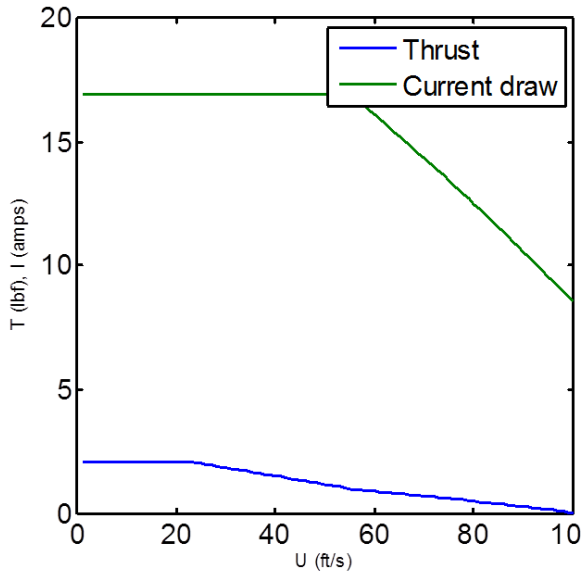

Figure 4.4.4b – Thrust and current draw

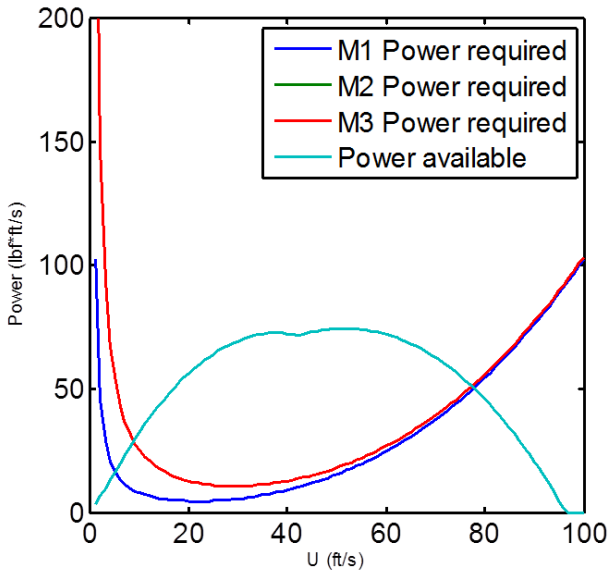

Figure 4.4.4c – Power required and available

4.5 Aerodynamic Characteristics

The aerodynamics subteam was responsible for systematically optimizing the aerodynamic characteristics of the aircraft to maximize competition score. This task included designing the wing, as well as predicting lift and drag characteristics using both analytical and numerical methods.

4.5.1 Airfoil selection

The airfoil cross-section has a great bearing on aerodynamic performance. The aerodynamics subteam used The Airfoil Investigation Database as the primary airfoil database and cross-referenced airfoils with airfoiltools.com. We began our search with 1,756 airfoils. To filter most of the extraneous airfoils, the following bounds were used.

- **Max C_L/C_D > 40:** to eliminate low efficiency airfoils
- **Max Thickness 7%-15%:** to remove extremely thin airfoils for the sake of manufacturability and eliminate thick airfoils which were generally less efficient. These percentages were based on past team experience and sample airfoils.
- **Max Camber < 9%:** to eliminate hyper cambered airfoils which would be difficult to manufacture.

These filtering criteria produced 742 airfoils. Of these airfoils, odd and uniquely shaped airfoils were removed due to the likelihood that they were designed for single point operating conditions or trans/super-sonic conditions. Additionally, airfoils with extremely sharp trailing edges were removed for manufacturability. From here, the remaining airfoils were evaluated for their merits at cruise and take-off conditions which were estimated at a Reynolds number of 200,000 and 100,000 respectively. Specifically, the airfoil needed to have a high $C_{L,max}$ and a high stall angle at takeoff, and at cruise an airfoil with a high glide ratio (C_L/C_D), and low C_{moment}. This left 21 airfoils which were either particularly outstanding in one aspect, or well-balanced in all categories.

In order to select a single airfoil representative of the entire wing, the following modified decision matrix (Figure 4.5.1a) was used. The weights were selected relative to the importance of each parameter towards competition score. Each airfoil was given a score by multiplying the weight by the corresponding normalized characteristic. The airfoils shown in Table 4.5.1b achieved the highest scores using this ranking system.

Weight	Characteristic
0.40	$C_{Lift,takeoffmax}$
0.25	$C_{Lift,max}/C_{Drag,max}$
0.20	$Stall_{AoA,Takeoff}$
0.15	C_{Moment}

Figure 4.5.1a – Modified Decision Matrix

MH 114 (13.02%)	SD7034	E385 (8.41%)	USA-35B	Eppler 68
0.66125	0.6378	0.6182	0.6082	0.6054

Table 4.5.1b Top Scoring Airfoils

$C_{Lift}\ vs.\ Angle\ of\ Attack$ and $C_{Lift}/C_{Drag}\ vs.\ Angle\ of\ Attack$ plots were created using the program XFLR5. The top performing airfoils are visibly shown in these plots (Figure 4.5.1c and 4.5.1d).

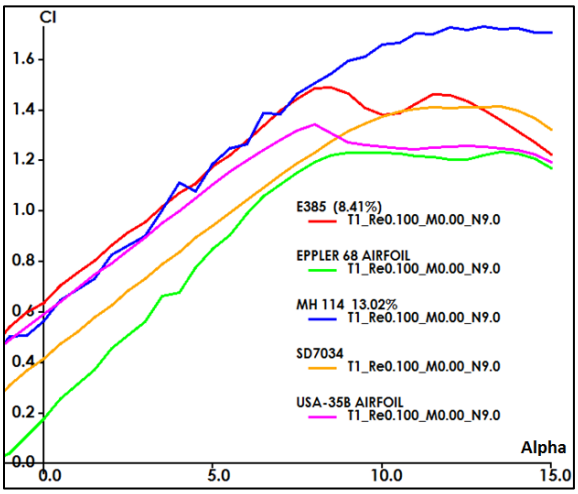

Figure 4.5.1c – C_L vs angle of attack

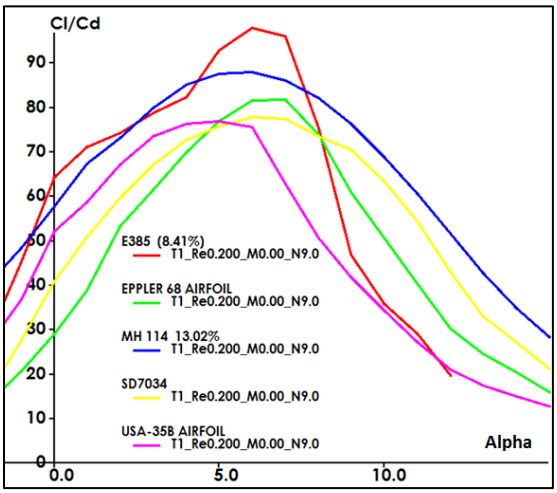

Figure 4.5.1d – C_L/C_D vs angle of attack

In order to find an accurate C_L for takeoff wing sizing, flaperon size and efficiency were analyzed. Within XFLR5, we created a series of flapped airfoils grouped according to their flap angle, from 35 to 50 degrees. In each group, we set the 5 different flap chords, from 40% to 20% of the wing chord. A collection of data from these calculations can be found in figure 4.5.1e. Analysis showed the best performing flap was at an angle of 40 degrees, with a length of 35% of the wing chord. We also observed that a flap chord of 20-30% of wing chord was enough to generate a CL within 10% of the optimal case. To accommodate other subteams, a flap chord of 25% and a flap angle of 40 degrees were chosen.

Flap angle	Group 1 (35°)	Group 2 (40°)	Group 3 (45°)	Group 4 (50°)
Hinge x-position				
60%	C_L = 2.00	C_L = 1.97	C_L = 1.99	C_L = 1.98
	Stall = 8°	Stall = 8°	Stall = 6°	Stall = 7°
65%	C_L = 2.03	C_L = 2.04	C_L = 2.01	C_L = 1.98
	Stall = 7.5°	Stall = 8°	Stall = 6°	Stall = 7°
70%	C_L = 2.02	C_L = 2.00	C_L = 1.99	C_L = 1.99
	Stall = 10°	Stall = 9°	Stall = 9°	Stall = 8°
75%	C_L = 2.03	C_L = 1.99	C_L = 1.98	C_L = 1.92
	Stall = 9°	Stall = 8°	Stall = 10°	Stall = 10°
80%	C_L = 1.96	C_L = 1.94	C_L = 1.90	C_L = 1.82
	Stall = 10°	Stall = 12°	Stall = 12°	Stall = 13°

Figure 4.5.1e – Potential flap positions

4.5.2 Wing design

In order to create an optimal wing, the competition flight score was translated into a set of wing parameters. These parameters resulted in tangible factors of wing design (twist, sweep, taper, and blending) that could be altered in order to optimize performance factors that drive competition score. Each of the mission score formulas were decomposed into a function of the variables, $C_D, b, c, and\ v_c$ (coefficient of drag, wing span, wing chord, and cruise velocity, respectively). Mission two score (M2) was held as a constant. The values for $n_{payloads}$, $N_{payloads}$, M_1, and T (number of payloads carried, maximum number of payloads carried, Mission 1 score, and minimum time for Mission 3, respectively) were found by averaging previous year's competition results. Constraints were added to the variables $C_D, b, c, and\ v_c$, as desired by the structures subteam and by the wing loading capability required for the missions.

With this wing parameter to score relationship, the team then systematically created 150 wings models that incorporated twist, sweep, taper, and blending. These were subject to takeoff constraints and were then run through XFLR5 to find the wing's performance characteristics. The resulting analysis found that the optimal wing, pictured in figure 4.5.2, would be a blending between MH114 at the base to MH116 at the tip with a 0.75 taper ratio.

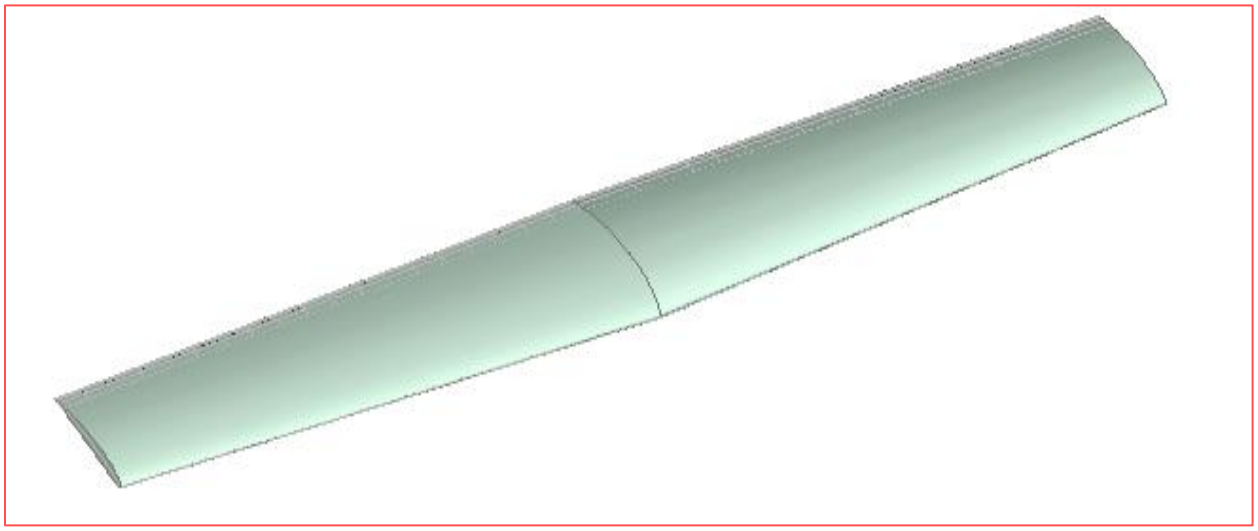

Figure 4.5.2 – Optimized wing aerodynamic design

4.5.3 Aerodynamic performance parameters

Validation of our wing design process was performed through the use of our mission model, which utilizes a set of calculations to estimate comprehensive aircraft performance parameters. These calculations are based on Shevell and Raymer's aircraft design texts, and are outlined in figure 4.5.3a.

Inputs			
Term	Description	**Term**	Description
ρ	Density of air (slug/ft^3)	$\bar{c}$	Mean aerodynamic chord (ft)
U	Airspeed (ft/s^2)	μ	Viscosity of air (slug/ft·s)
a_o	2D airfoil lift curve slope (1/degrees)	u	Correction for non-elliptic loading
AR	Aspect ratio	s	Fuselage correction factor
a_{ZL}	Angle of attack for zero lift (degrees)	S	Planform area (ft^2)
$m.t.$	Maximum airfoil thickness (%)	C_{DpLG}	Landing gear parasite drag
d_f	Diameter of fuselage (ft)	L_f	Length of fuselage (ft)

Formulas	
$q = 0.5\rho U^2$	Dynamic pressure (lbf/ft^2)
$C_{La,w,h} = a_0/(1 + 5.73(a_0/\pi AR_{w,h}))$	3D airfoil lift curve slope (1/degrees)
$C_{L,w,h} = C_{La,w,h}(\alpha - \alpha_{ZL,w,h})$	Lift coefficient
$L = C_{Lw}qS_w + C_{Lh}qS_h$	Lift from wing and tail (lbf)
$K_{w,h} = 1 + 2.61(m.t./100)$	Wing and tail parasite pressure drag correction factor
$K_f = 1.4 - 0.05(L_f/D_f)$	Fuselage parasite pressure drag correction
$Re = \rho U\bar{c}/\mu$	Reynolds number
$C_f = 1.328/\sqrt{Re}$	Skin friction coefficient (laminar flow)
$C_{Dp,w,h} = 2KC_f$	Wing and tail parasitic drag
$D_{Dpf} = K_f C_f$	Fuselage parasitic drag
$k_{w,h} = 0.38C_{Dp}$	Wing and wail induced pressure drag correction factor
$C_{D,w,h} = [k + (\pi ARus)^{-1}]C_L^2 + C_{Dp}$	Wing and tail drag coefficient
$C_{DpLG} = \frac{1}{4}(frontal\ area)/S_w$	Landing gear drag coefficient
$D = (C_{Dw} + C_{DpLG} + C_{DpST})qS_w + C_{Dh}qS_h + C_{Dpf}qS_f$	Drag from wing, tail, fuselage, landing gear and external stores (lbf)

Figure 4.5.3a – Lift and drag mission model calculations

Figure 4.5.3b outlines the results of these calculations which serve as estimates for overall aircraft aerodynamic performance.

Flight Phase	Lift (lbf)	Drag (lbf)	L/D	Angle of Attack (°)	Airspeed (ft/s)
Takeoff	4.06	0.45	8.99	7.0	32.0
Cruise	4.06	0.63	6.42	-3.0	77.3

Figure 4.5.3b – Aircraft lift and drag characteristics (Mission model simulation)

4.5.4 – Lift and drag simulation

Further verification of the lift and drag performance of our aircraft was facilitated by the use of ANSYS/FLUENT computational fluid dynamics simulations. The implementation of this software allows us to simulate the airflow around an approximate 3D model of our aircraft, as shown in figure 4.5.4a.

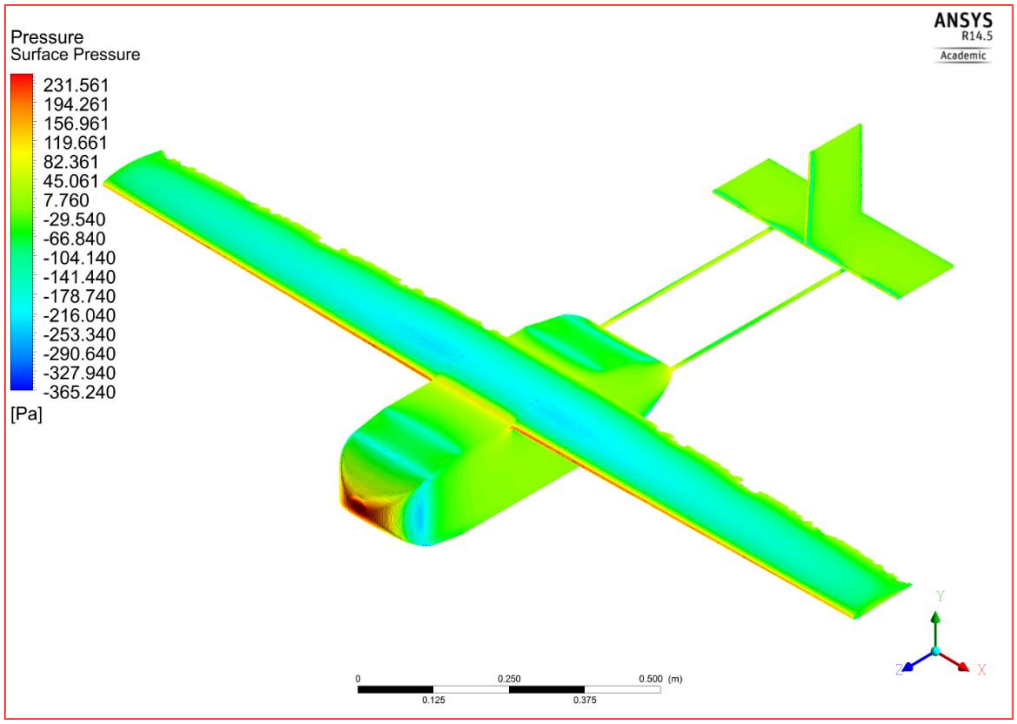

Figure 4.5.4a – Aircraft surface pressure distribution at cruise velocity

Figure 4.5.4b tabulates the total lift and drag from the simulation at our critical operation conditions. Discrepancies are small and related to the fuselage lift and drag contributions. The mission model used in section 4.5.3 does not account for fuselage lift and assumes that the fuselage is a cylinder. However, the magnitude of these discrepancies are easily overcome by our design factors of safety.

Flight Phase	Lift (lbf)	Drag (lbf)	L/D	Angle of Attack (°)	Airspeed (ft/s)
Takeoff	4.35	0.49	8.87	7.0	32.0
Cruise	3.91	0.70	5.59	-3.0	77.3

Figure 4.5.4b – Aircraft lift and drag characteristics (CFD simulation)

4.6 Stability Characteristics

The stability and controls subteam was responsible for ensuring that the aircraft exhibits handling characteristics necessary to complete the missions and land safely. This task was accomplished through the sizing of the tail and control surfaces. Iteration was crucial to the sizing of the horizontal and vertical tail as well as the control surfaces. A MATLAB script was written utilizing equations for static and dynamic stability about all three axes from Caughey. Raymer's prescribes were utilized to size control surfaces. Inputs to the script include the aircraft geometry, atmospheric conditions, and initial conditions for dynamic simulations. The script then calculates and outputs the static margin, elevator deflection necessary to maintain angle of attack, and dynamic response to simulated flight perturbations.

4.6.1 Longitudinal static stability and control

The tail was sized by firstly inputting an initial geometry for the wing, fuselage, and horizontal tail. The resultant static margin and elevator deflection, found using calculations in figure 4.6.1a and figure 4.6.1b, revealed whether the aircraft was longitudinally stable and able to be trimmed. We found, through various iterations, that increasing the distance between the wing apex and the tail apex and moving the C.G. forward were the best methods for increasing the static margin and decreasing the elevator deflection required to trim the aircraft. The team iterated across several geometries and CG positions to optimize necessary elevator deflection and static margin, ultimately providing the final sizing for the elevator and horizontal stabilizer.

Major Values Involved	
Variable	**Description**
AR	Aspect ratio (for wing and tail)
λ	Taper ratio (for wing and tail)
T_{a_0} W_{a_0}	Tail's and Wing's airfoil's lift curve slope
Λ_{c_4}	Sweep angle at quarter cord (for wing and tail)
W_S T_S	Wing's and Tail's reference area
$\bar{c}$	Wing's mean chord
η V_H	Tail's effectiveness and volume parameter
$\frac{\partial \epsilon}{\partial \alpha}$	The effect of downwash due to the wing
X_{CG}	Wing and horizontal tail geometry values
V_f	Volume of the fuselage
Formulas	
$C_{L_{\alpha_t}} = \frac{\pi * AR_t}{1 + \sqrt{(1 + (\frac{\pi * AR_t}{T_{a_0} * \cos \Lambda_{t_{c4}}})^2 \cdot (1 - M^2 * \cos {\Lambda_{t_{c4}}}^2)}}$	Tail lift coefficient with respect to angle of attack
$C_{L_{\alpha_w}} = \frac{\pi * AR_w}{1 + \sqrt{(1 + (\frac{\pi * AR_w}{W_{a_0} * \cos \Lambda_{c_4}})^2 * (1 - M^2 * \cos {\Lambda_{c_4}}^2)}}$	Wing lift coefficient with respect to angle of attack
$C_{L_\alpha} = C_{L_{\alpha_w}} + C_{L_{\alpha_t}} * \eta * \frac{T_S}{W_S}\left(1 - \frac{\partial \epsilon}{\partial \alpha}\right)$	Aircraft's lift coefficient with respect to angle of attack
$C_{m_{\alpha_f}} = \frac{2 * V_f}{W_S * \bar{c}}$	Fuselage moment coefficient with respect to angle of attack
$X_{NP} = 0.25 + \frac{\eta * V_H * C_{L_{\alpha_t}} * \left(1 - \frac{\partial \epsilon}{\partial \alpha}\right) - C_{m_{\alpha_f}}}{C_{L_\alpha}}$	Neutral Point (% of root mean cord of the wing)
$S.M. = \left(\frac{X_{NP}}{\bar{c}} - \frac{X_{CG}}{\bar{c}}\right)$	Static Margin (% of root mean cord of the wing)

Figure 4.6.1a – Static Margin Calculations

Figure 4.6.1b, in addition to outlining elevator deflection calculations, contains the equations necessary to define the coefficient of moment due to the fuselage, wing, and tail. Summing these coefficients of moment gives the coefficient of moment for the entire aircraft.

Values Involved (aforementioned variables not included)	
Variable	Description
α	Angle of Attack at which to calculate coefficient of moment for the aircraft and the necessary elevator deflection for trim
α_0	Angle of attack for zero lift on the aircraft
ϵ_0	Angle of downwash coming off the wing
i_t	Incidence angle of the horizontal tail
$C_{L_{0_w}}$	Coefficient of lift due to the wing at zero angle of attack
$C_{m_{ac_w}}$	Coefficient of moment about the aerodynamic center of the wing

Formulas	
$C_{m_{0_w}} = C_{m_{ac_w}} + C_{L_{0_w}} * (\frac{X_{cg}}{\bar{c}} - \frac{X_{ac}}{\bar{c}})$	Coefficient of moment due to the wing at zero angle of attack
$C_{m_{0_t}} = -\eta * V_H * C_{L_{\alpha_t}} \left(i_t - \varepsilon_0 + \left(1 - \frac{d\varepsilon}{d\alpha}\right) \right) * \alpha_0$	Coefficient of moment due to the tail at zero angle of attack
$C_{m_{0_f}} = C_{m_{\alpha_f}} * \alpha_0$	Coefficient of moment due to the fuselage at zero angle of attack
$C_{m_0} = C_{m_{0_w}} + C_{m_{0_t}} + C_{m_{0_f}}$	Coefficient of moment of the aircraft at zero angle of attack
$C_{m_\alpha} = \left(\frac{X_{cg}}{\bar{c}} - \frac{X_{ac}}{\bar{c}}\right) * C_{L_{\alpha_w}} - \eta * V_H * C_{L_{\alpha_t}} * \left(1 - \frac{d\varepsilon}{d\alpha}\right) + C_{m_{\alpha_f}}$	Coefficient of moment with respect to angle of attack of the aircraft
$C_{m_{cg}} = C_{m_0} + C_{m_\alpha} * \alpha$	Coefficient of moment of the aircraft about the center of gravity
$\tau = f\left(\frac{control\ surface\ area}{lifting\ surface\ area}\right)$	Flight effectiveness parameter (empirical formula)
$C_{m_{\delta_e}} = -\tau * V_H * \eta * C_{L_{\alpha_t}}$	Coefficient of moment due to elevator deflection
$\delta_e = -\frac{C_{m_{cg}}}{C_{m_{\delta_e}}}$	Necessary elevator deflection to counter coefficient of moment of the aircraft

Figure 4.6.1b – Coefficient of Moment and Elevator Calculations

Figure 4.6.1c shows the resultant moment coefficients for aircraft components. It's important to note that coefficient of moment's slope for the entire aircraft is negative, indicating longitudinal static stability. The elevator deflection vs. angle of attack in figure 4.6.1d shows us that the aircraft can be effectively trimmed. Note that positive elevator deflection is defined as downward.

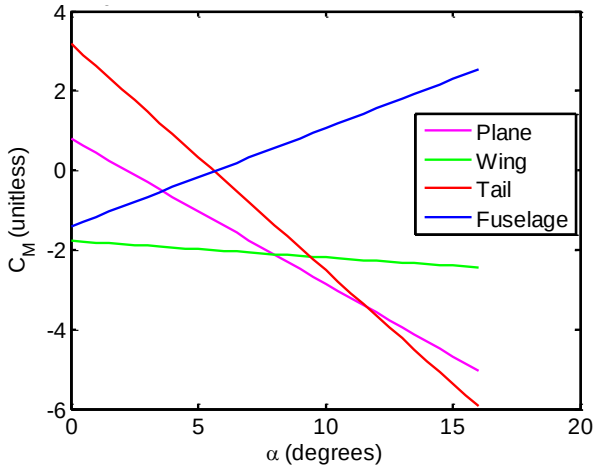

Figure 4.6.1c – Coefficients of moment

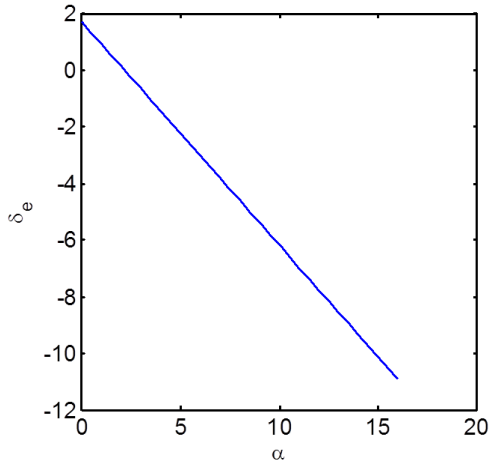

Figure 4.6.1d – Required elevator deflection at AoA (°)

Finally, figure 4.6.1e outlines the longitudinal stability performance parameters of the final tail design. A relatively large static margin is utilized to ensure stable flight in the often gusty conditions of Wichita, Kansas.

Parameter	Static Margin	Elevator trim for 0° AoA	Elevator trim for 7° AoA
Value	21.99%	2°	-6°

Figure 4.6.1e – Longitudinal static stability performance parameters

4.6.2 Lateral and directional static stability and control

The vertical tail was next sized to have a reference area proportional to that of the horizontal tail's reference area as outlined in Figure 4.6.2. Both the horizontal tail's and vertical tail's reference area can be sized using estimates in Raymer. The ratio of these suggested reference areas was used in order to produce the vertical tail's required reference area.

Values Involved	
Variable	Description
c_{HT}	Raymer's horizontal tail volume coefficient
c_{VT}	Raymer's vertical tail volume coefficient
L_{HT}	Distance between aerodynamic center of horizontal tail and wing
L_{VT}	Distance between aerodynamic center of vertical tail and wing
T_S	Actual horizontal tail area sized earlier
W_b W_S $\bar{c}$	Wing's span, reference area, mean chord
Formulas	
$S_{VT} = \frac{c_{VT} * W_b * W_S}{L_{VT}}$	Raymer's suggested vertical tail area
$S_{HT} = \frac{c_{HT} * \bar{c} * W_S}{L_{VT}}$	Raymer's suggested horizontal tail area
$S_{V_{approx}} = T_S * \frac{S_{VT}}{S_{HT}}$	Approximate vertical tail area using ratio of Raymer's suggested tail size

Figure 4.6.2 – Coefficient of Moment and Elevator Calculations

The rudder and flaperons were also sized according to Raymer's prescribes. The rudder was sized to be approximately 23% the area of the vertical tail while the flaperon was sized to have a chord length of 25% that of the wing. A high wing design was chosen to ensure adequate lateral stability through a "keel effect". All control surfaces were chosen to be full span for increased manufacturability.

4.6.3 Dynamic stability

Dynamic stability of the aircraft was also verified through a series of MATLAB simulations in order to ensure that our aircraft quickly reaches steady state conditions during flight. Figure 4.6.3a shows the results of stability derivative calculations, while figures 4.6.3b and 4.6.3c show example simulations of longitudinal and lateral/directional perturbations, respectively. With this analysis, the longitudinal stability of the aircraft was verified for various perturbations in the state variables of speed, angle of attack, pitch rate, and pitch angle. The lateral/directional stability analysis allowed us to also simulate perturbations in sideslip, roll angle, roll rate, and yaw rate. These results confirm the stability of our aircraft.

Sideslip		Roll Rate		Yaw Rate	
C_{y_β}	-0.8608	C_{y_p}	-0.0421	C_{Y_r}	0.2909
C_{l_β}	-0.0726	C_{l_p}	-0.8776	C_{l_r}	0.1828
C_{n_β}	0.1337	C_{n_p}	-0.0226	C_{n_r}	-0.3627
Angle Of Attack		**Pitch Rate**			
C_{L_α}	4.9949	C_{Z_q}	-4.8666		
C_{M_α}	-1.1981	C_{M_q}	-21.3606		

Figure 4.6.3a – Calculated stability derivatives

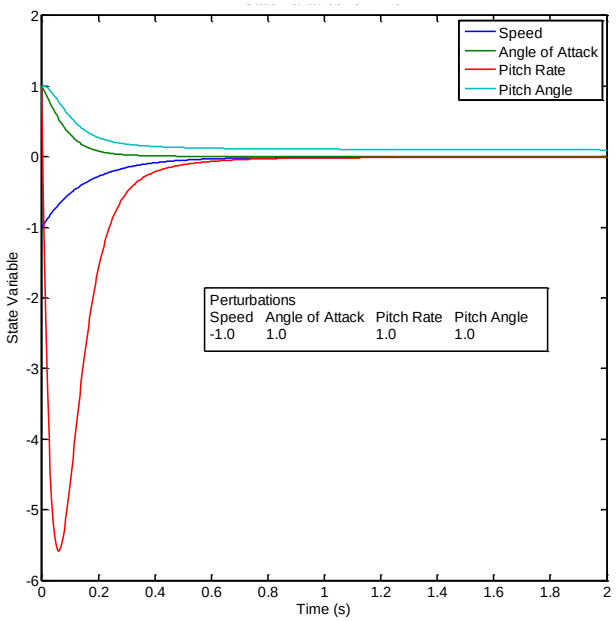

Figure 4.6.3b – Longitudinal simulation

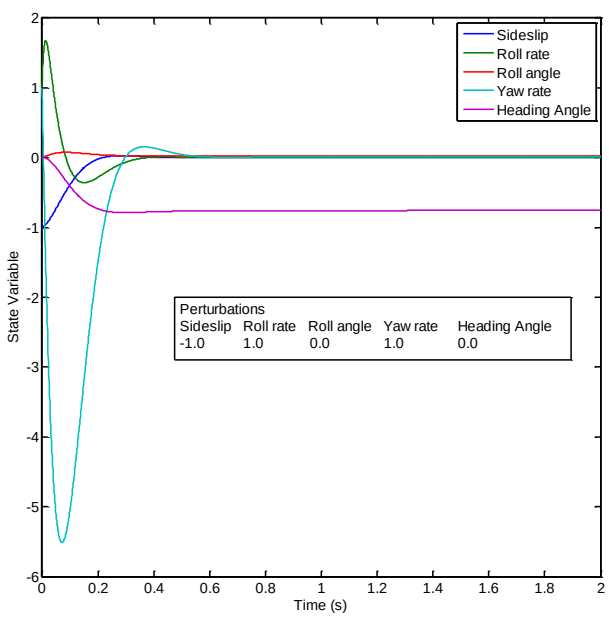

Figure 4.6.3c – Lateral/Directional simulation

4.7 Mission Performance Estimates

Figure 4.7.1 provides estimates for the performance of the aircraft in each of the three missions. We utilized our mission model with the developed estimates for system performance and aircraft geometry to calculate the values for our aircraft. The estimate of maximum payloads carried is based on the additional structure and aircraft volume necessary to accommodate payloads. Our estimates for best flight speeds in missions one and three are based on past competition experience and propulsion system limitations.

Mission 1		Mission 2		Mission 3	
Laps completed	7	Payloads carried	2	Time flown	112
Max laps completed	8	Max payloads carried	5	Min time flown	100
M1 score	**1.75**	M2 score	**1.6**	M3 Score	**5.35**

Figure 4.7.1 – Estimated mission performance

5 Detailed Design

In the following section of this report, we document the dimensional and performance parameters, structural characteristics, and systems design, selection, and integration of the final aircraft design. The detailed design process embodies our primary objective of minimizing structural weight.

5.1 Dimensional Parameters

Figure 5.1 lists the pertinent dimensional parameters of the final aircraft design. It includes overall aircraft dimensions and dimensions of key subsystems.

		Horizontal Tail		Fuselage	
		Span	17"	Length	24.7"
Overall Dimensions		MAC	3.5”	Width	7.2"
Length	48.3"	Area	59.5"	Height	8.0"
Width	69.2"	Airfoil	Flat Plate	**Main Landing Gear**	
Height	11.4"	Incidence	0.00°	Length	0.375"
Wing		**Vertical Tail**		Width	1.5"
Span	69.2"	Span	7"	Height	7.1"
MAC	6.6”	MAC	3.25”	Wheel diameter	2.15"
Area	408 in^2	Area	45.5"	**Ground AoA**	
Aspect Ratio	9.4	Airfoil	Flat Plate	0^o	
Airfoil	MH114/116	Wing apex to horizontal tail apex distance			30”
Incidence	0.00°	Wing apex to vertical tail apex distance			30”
Flaperons (2)		**Elevator**		**Rudder**	
Span	31.0"	Span	17.0"	Span	7.0"
Percent Chord	25%	Percent Chord	25%	Percent chord	26%
Maximum defl.	40°	Maximum defl.	25°	Maximum deflection	20°

Figure 5.1 – Dimensional Parameters of Final Design

5.2 Structural Characteristics

The table below summarizes the structures subteam’s design goals as they relate to overall design requirements. We sought to minimize the structural weight of the aircraft while providing adequate strength and rigidity for high wing loading during turns and the shock impact of landing.

Overall Design Requirements	Subteam Design Requirements
Minimize weight	Minimize airframe structure
Hold two Mission II payloads	Design attachments to accommodate two internal stores
Minimize drag	Maintain aerodynamic profile and proper blending between components

Figure 5.2 – Structures Design Requirements

5.2.1 Load paths

Two hollow carbon fiber tubes .281 inches in diameter run the length of the aircraft. A single .375 inch tube runs along most of the wing, before telescoping down to a .281 inch tube near the tips of the wing. The two fuselage booms run through a hard plastic bulkhead near the center of the fuselage. This same bulkhead provides the attachment point between the wing, fuselage, and landing gear, adding further support. The rear landing gear is designed to take the gross majority of the load when landing. For this reason, the center of gravity is placed very near to the rear landing gear column.

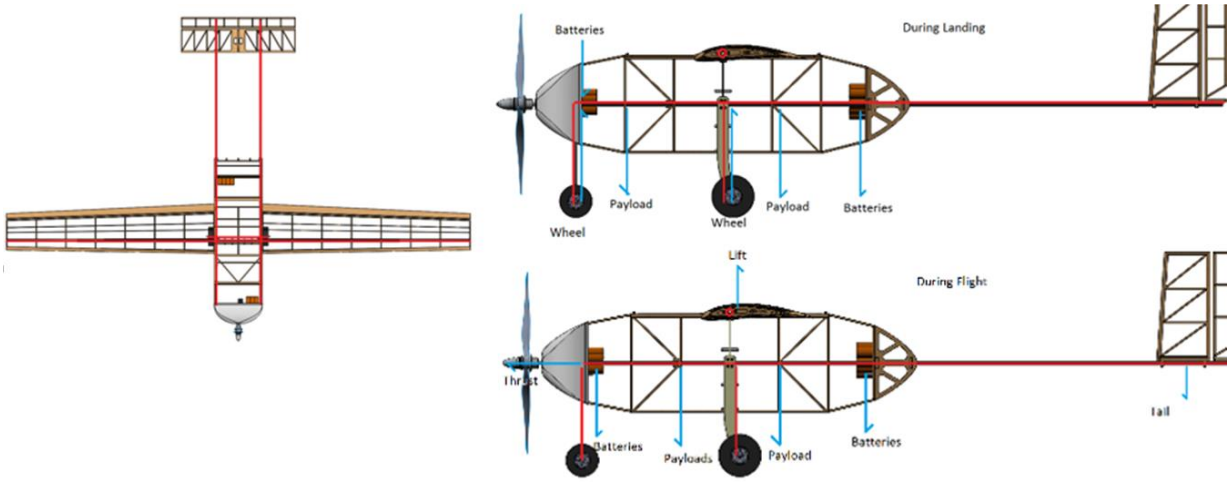

Figure 5.2.1 – Load Paths

5.2.2 Structural analysis

In order to size the wing spar appropriately, both a simplified model and a more complex ANSYS model were created. For the simplified model, the material was assumed to be isotropic and basic static analysis was performed. The results for a fully loaded aircraft (a total of 4 pounds) undergoing a 2.5 G turn are illustrated in figure 5.2.2a (with the selected spar size). The test value of 2.5 Gs was chosen to simulate the loading conditions of a banked turn and because it is roughly equal to the wing-tip load test performed during technical inspection.

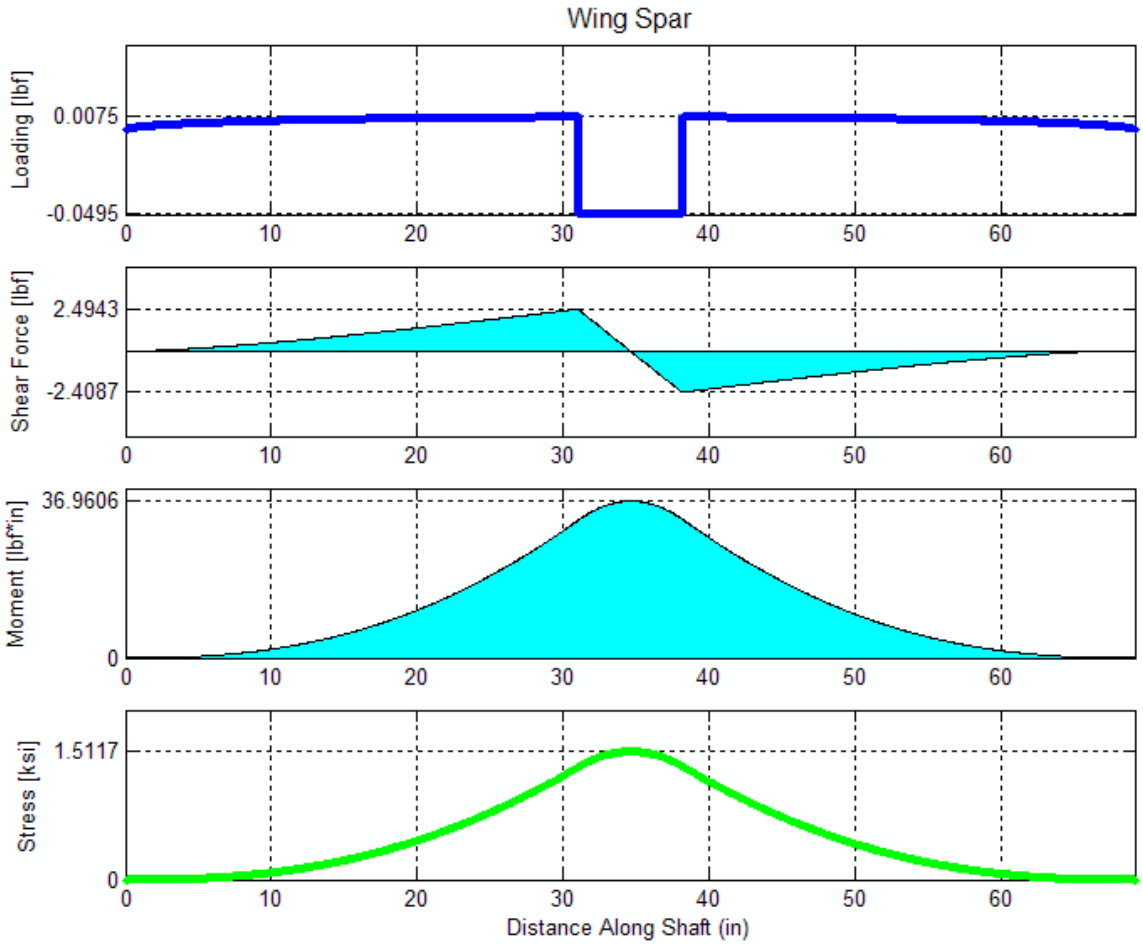

Figure 5.2.2a – Simplified Loading on the Wing Spar

Using the yield stress of carbon fiber it was possible to solve for the safety factor. At these specifications it is 19.86. Given the fact that large assumptions are being made, we chose to perform physical testing before attempting to further reduce the main spar diameter.

We also used ANSYS for further analysis. Because carbon fiber is an anisotropic material, we inputted several sizes of pultruded carbon fiber tube from our supplier and ran an ANSYS simulation to find the deflection at 2.5 Gs. Additionally, using geometric arguments and the material properties for balsa, the maximum amount of allowed deflection before the balsa wing components would break was found. All of this data is presented in figure 5.2.2b, where the dots represent tube sizes and the dashed line is the maximum acceptable deflection of the balsa. The dots have been color coded for acceptability, and the selected point for our prototype has been labeled on the plot. Note that the selected point is the same size as the spar used in the above, simpler calculations.

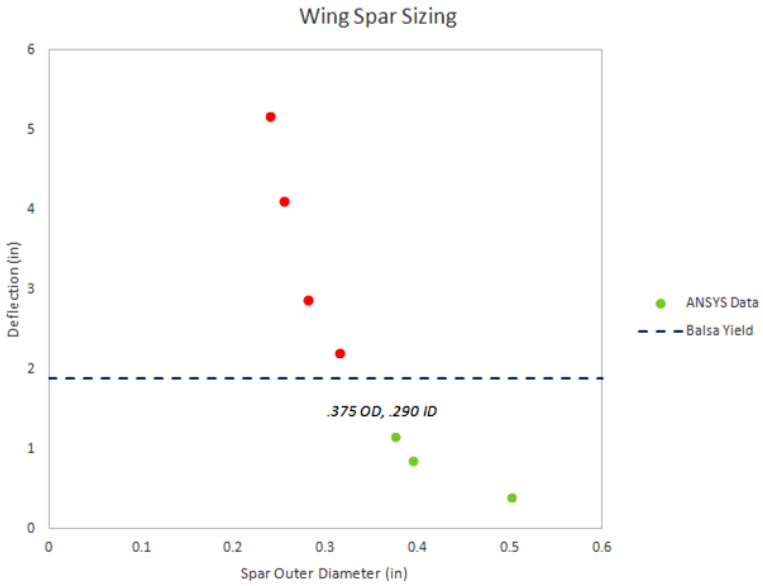

Figure 5.2.2b – Wing Spar Sizing using ANSYS

Figure 5.2.2c shows a visualization of one case in out ANSYS analysis simulation (simple cantilevered beam of an anisotropic material):

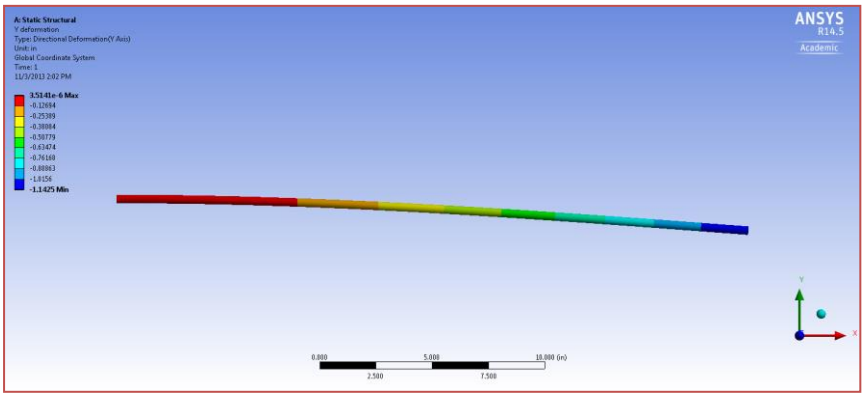

Figure 5.2.2c – ANSYS visualization

5.3 Aircraft Systems Design, Component Selection and Integration

This section of the report describes the design, selection, and integration of the aircraft's key subsystems. The components discussed include the fuselage, wing, wing mount system, access hatch, empennage, nose cone, and electronics.

5.3.1 Fuselage design

The design of the fuselage revolved around keeping the empty weight low above all else. In order to do this, a design involving a very lightweight profile held together with a series of strong "skeleton" spars was developed. The entire design is dependent on a central fiberglass reinforced epoxy bulkhead.

This singularly supports all types of payloads and well as two longitudinal booms which run down the length of the aircraft. It also serves as the attachment point for the wing and the main landing gear. Attached to the front of the longitudinal booms is a spruce bulkhead to which the motor, most of the electronics, and the nose gear attach. At the end of the fuselage is another smaller spruce bulkhead; the batteries are split between these two spruce bulkheads. The rest of the fuselage is constructed with lightweight balsa beams, which serve only to define the shape of the aircraft.

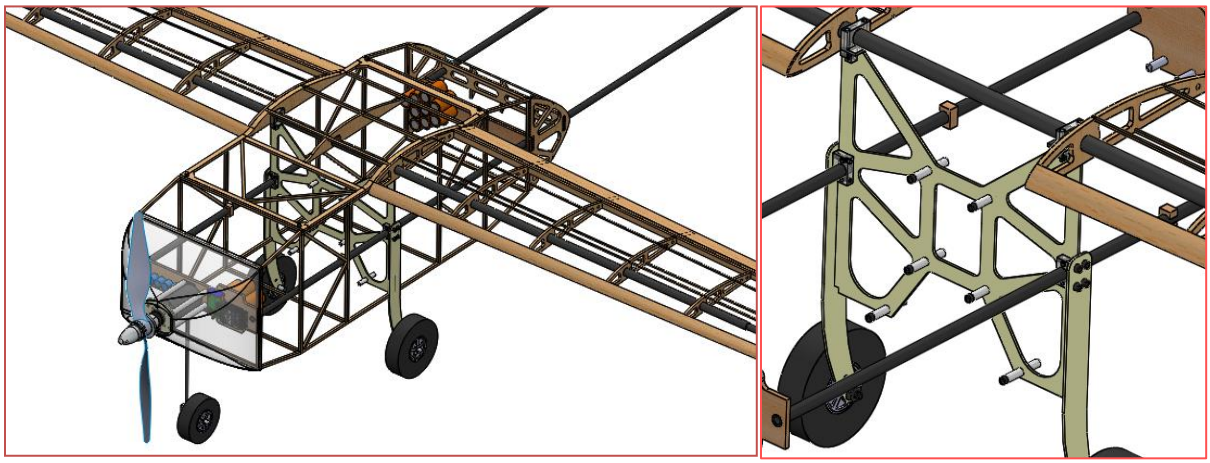

Figure 5.3.1 – Fuselage Design and Main Structural Bulkhead

5.3.2 Payload access hatch design

The payload access hatch serves as the single point of entry into the fuselage. The hatch also acts as a blended central section between both sides of the wing in order to preserve the aerodynamic profile of the aircraft. It is held in place by four screws in the corners of the hatch.

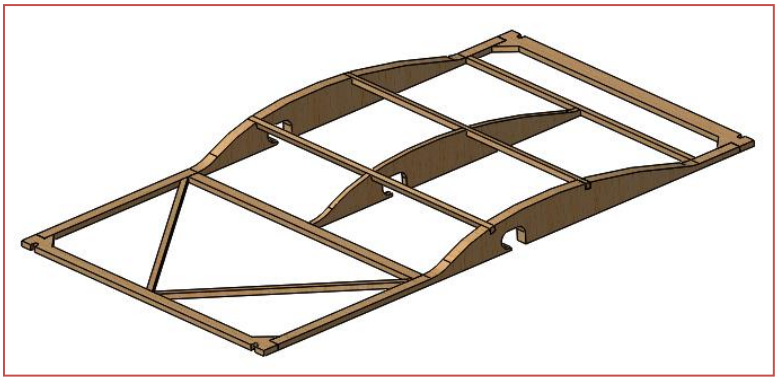

Figure 5.3.2 – Payload Access Hatch

5.3.3 Wing design

The wing and flaperon design is a balsa build-up consisting of ribs and stringers. At quarter-chord are two carbon fiber spars to increase rigidity; there is a larger .375” diameter spar in the center section, which decreases to a .281” diameter spar at the wing tips. This was done because the additional strength

of the larger spar is not required at the far ends of the wings. Also note that the larger spar passes through two polycarbonate blocks which allow for attachment to corresponding blocks on the fuselage.

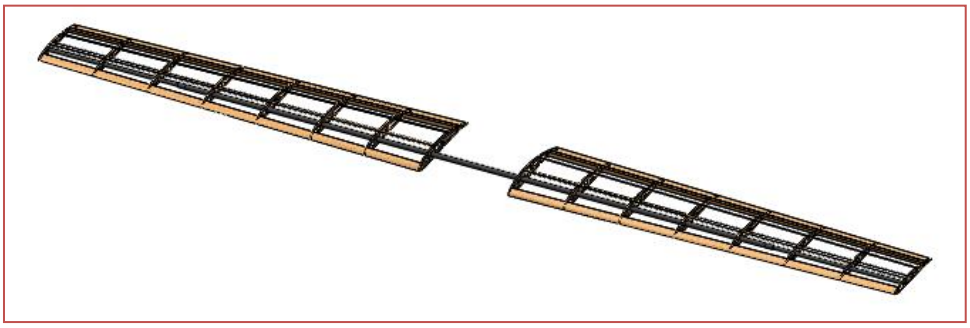

Figure 5.3.3 – Wing Design

5.3.4 Wing attachment design

In order to properly secure the wing assembly to the fuselage and keep it removable for easier transportation, an attachment system was designed to maximize both strength and ease of use. Two pairs of polycarbonate blocks were machined to be firmly glued to the wing spar and the central bulkhead. These blocks can then be attached together with small aluminum screws.

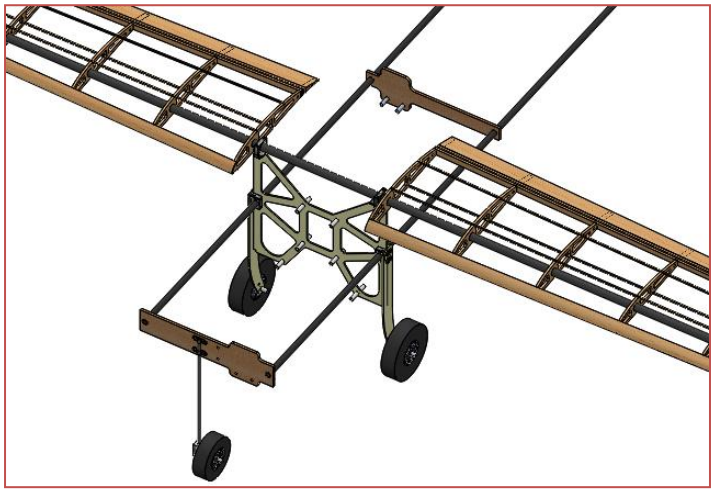

Figure 5.3.4 – Wing to Fuselage Attachment

5.3.5 Empennage design

We aimed for a minimalist empennage design to reduce weight. It is constructed completely of balsa, with care taken to align all of the struts with the grain of the wood for enhanced strength. Furthermore, the two spar design of the fuselage prevents the tail from twisting during flight. The servo wires for the tail are fed through the supporting booms in order to preserve the aerodynamics of the aircraft.

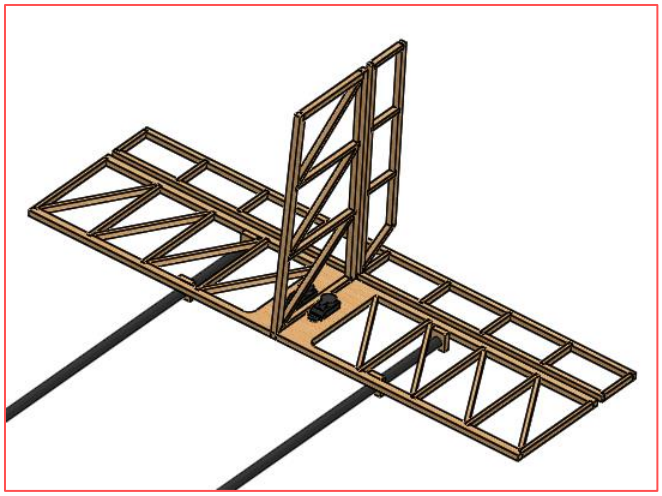

Figure 5.3.5 – Tail Design

5.3.6 Nosecone design

The nosecone was designed to provide space for all electronics mounted on the front spruce bulkhead, to provide an aerodynamic profile, and to be as light as possible. It is attached by a single set of screws on the front, positioned just above and below the propeller. As it offers no support to any components, it is constructed out of vacuum molded plastic, which is a lighter and simpler alternative than the carbon fiber used by the team in previous years.

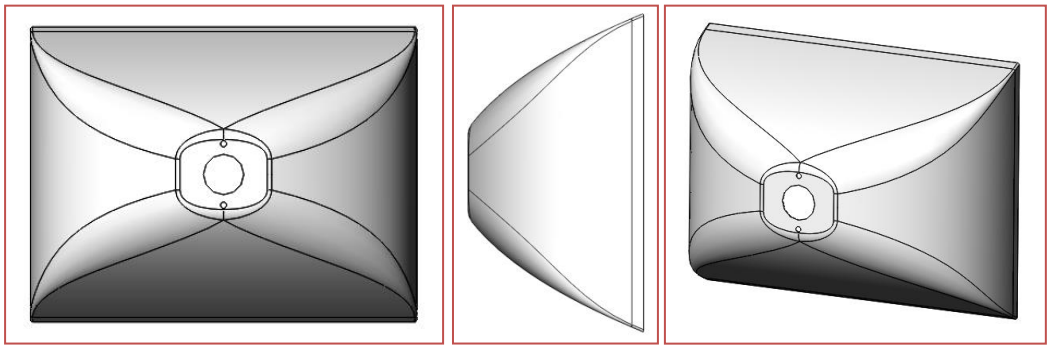

Figure 5.3.6 – Nosecone Design

5.3.7 Landing gear design

The main gear is attached directly to the longitudinal spars and the central bulkhead at the same time to ensure a safe landing. The nose gear is attached to the front bulkhead. A single front gear is centered below the nosecone. Note that this gear is not steerable as it would only add weight and we found it unnecessary to be so during testing with the simulated rough terrain. Lightweight and small-profile skids are also being researched as a possible alternative to the rear wheels.

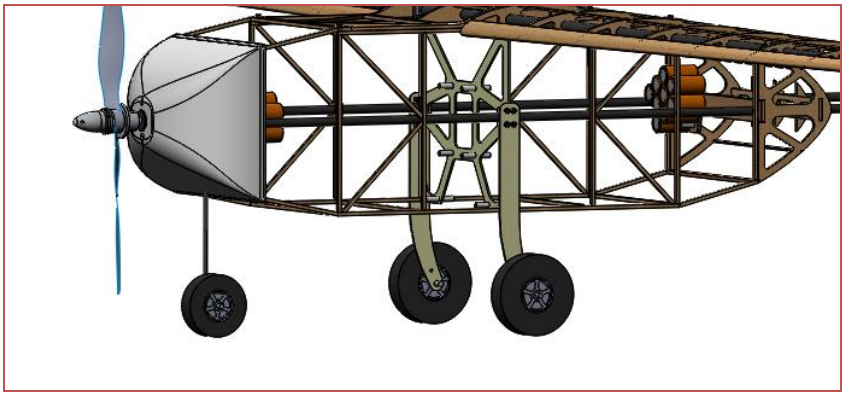

Figure 5.3.7 – Landing Gear

5.3.8 Electronics selection

All auxiliary electronic components were selected to be as lightweight as possible while meeting minimum requirements. These components are shown in figure 5.3.8. The Futaba servo is the lightest servo in its class, designed to operate in aircraft of our scale. The KAN 125 receiver battery is being used due to its lightweight and our team's success with it in the past. Our castle creations ESC is one of the lightest and most efficient on the market. Finally, Spektrum's AR8000 receiver is the smallest and lightest receiver that provides the required failsafe programmability.

Picture	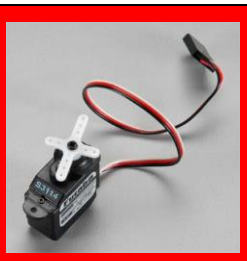			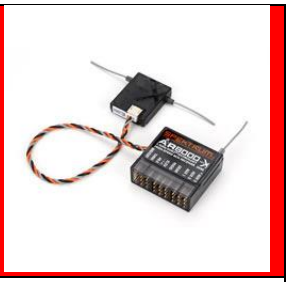
Component	Servo Motor	Receiver Battery	Electronic Speed Controller (ESC)	Receiver
Name	Futaba S3114	KAN 125	Castle Creations Talon 25	Spektrum AR8000

Figure 5.3.8 – Selected electronic components

5.4 Payload System Design

As discussed in section 4.2.1, we chose to carry two of the Mission II payloads so that we could sufficiently minimize the weight of the aircraft. In our design, both mission sets of payloads are held in place by securing them to the central bulkhead. This is done though a system of straps and adjustable pegs. The pegs act as small feet to secure the payloads vertically and horizontally. They are also adjustable to be able to accommodate the different sized payloads between the two payload missions. The straps act as the final tie down, making sure that the payloads cannot shift during flight. The straps have been oriented parallel to the fuselage to ensure easy installation of the payloads.

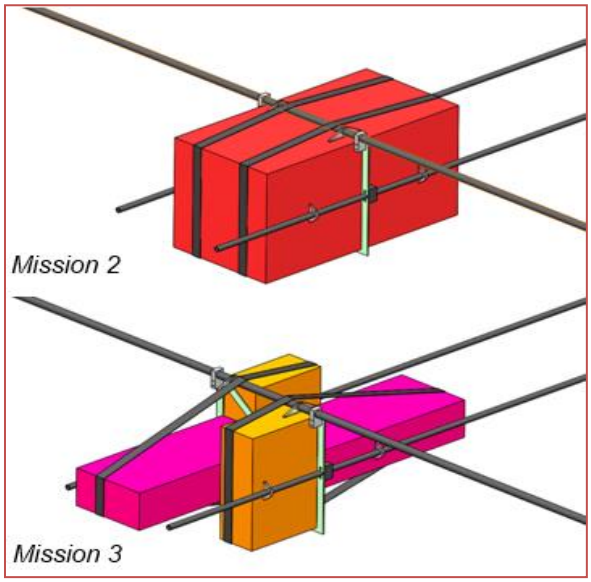

Figure 5.4 – Secure Payload System

5.5 Aircraft Component Weight and Balance

Figure 5.5a lists the breakdown of the aircraft's empty weight by system and subsystem. A majority of the weight comes from the electronics rather than the structural airframe. The direction of the axes and the position of the origin are displayed in figure 5.5b.

Component		Qty.	Weight (lbf)	CG Moment Bal. (ft*lbf)		Total (lbf)
				X	Z	
Structures	Fuselage	1	0.283	0	-0.14	0.785
	Landing Gear	1	0.147	0	0.012	
	Nosecone	1	0.058	0	0.047	
	Tail	1	0.041	0	-0.11	
	Wing	1	0.257	0	-0.025	
Controls	Receiver	1	0.0088	-0.0018	0.0065	0.051
	Receiver Battery	1	0.026	0.0048	0.017	
	Servos	4	0.016	0	-0.022	
Propulsion	Motor Assembly	1	0.3929	0	0.34	1.220
	Propeller	1	0.0638	0	0.066	
	Main battery	2	0.726	0.020	-0.23	
	Speed Controller	1	0.0375	-0.0043	0.027	
Payloads	Mission 2	2	1	0	-0.09	2.0
	Mission 3	3	.05	0	-0.10	
Totals	Empty			**0.0188**	**-0.0108**	**2.056**
	Mission 2			**0.0188**	**-0.1008**	**4.056**
	Mission 3			**0.0188**	**-0.1108**	**4.056**

Figure 5.5a – Component Weights and Moments about the CG

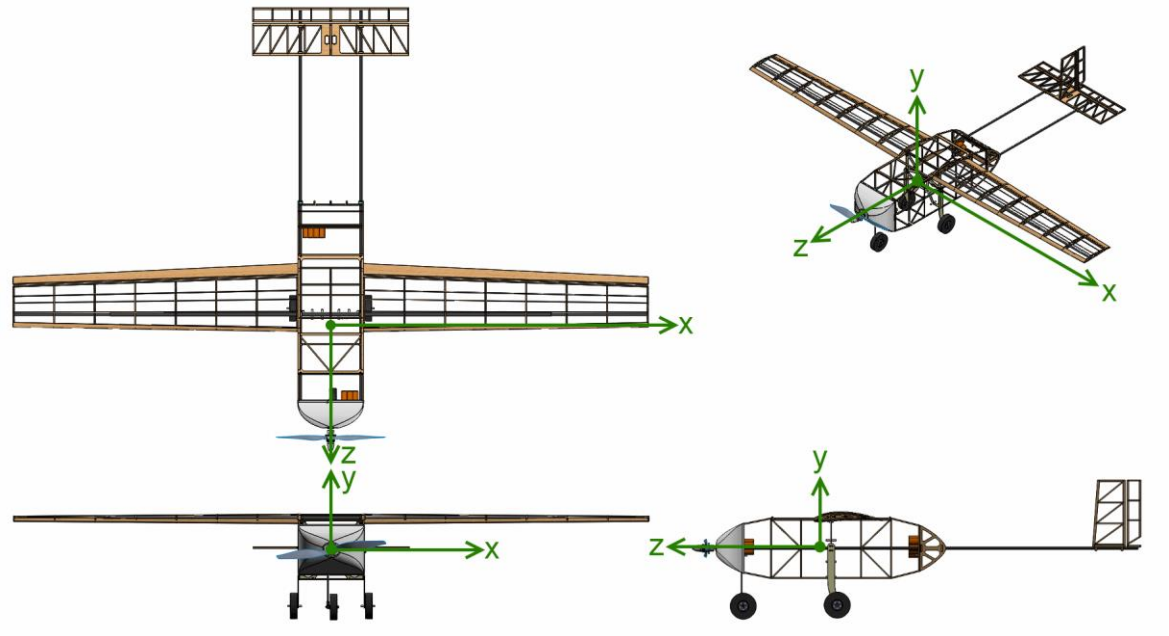

Figure 5.5b – Center of gravity diagram

5.6 Flight Performance Parameters

Listed below are the relevant flight performance parameters calculated by the mission model for each of the competition's three flight missions. The values shown reflect the final weight and geometry estimates developed during the detailed design phase.

Parameter	Mission I	Mission II	Mission III
C_{Lmax}	1.52	1.52	1.52
$C_{Ltakeoff}$	1.24	1.33	1.33
$C_{Lcruise}$	0.22	0.38	0.38
C_{D0}	0.052	0.052	0.052
$(L/D)_{takeoff}$	8.99	8.99	8.99
$(L/D)_{cruise}$	3.79	6.42	6.42
Stall Speed (ft/s)	7.2	10.7	10.7
Takeoff Speed (ft/s)	25.5	32.0	32.0
Takeoff Distance (ft)	10.0	37.0	37.0
Takeoff Angle (degrees)	7.0	7.0	7.0
Cruise Speed (ft/s)	77.3	76.1	76.1
Cruise Angle (degrees)	-4.6	-3.0	-3.0
Turn Rate (degrees/s)	141	82.2	82.2
Max. Load Factor	5.0	3.0	3.0
Wing Loading (lbf/ft^2)	0.73	1.43	1.43
Total Flight Time (s)	225	114	114
Gross Weight (lbf)	2.06	4.06	4.06

Figure 5.6 – Aircraft Flight Performance Parameters

5.7 Mission Performance Summary

Figure 5.7 documents the aircraft's performance for each of the three flying missions and for each of the phases of flight modeled.

Mission I					
Flight Phase	Qty.	Final Speed (ft/s)	Distance (ft)	Time (s)	Capacity (mAh)
Takeoff	1	25.5	10	0.5	2.9
Climb	1	55.7	41	7.9	34.8
First Leg	1	65	80	1.3	5.2
Cruise	6.67	77.3	1640	21.2	64.8
180 turn	14	64.1	-	1.3	4.7
360 turn	7	64.1	-	2.6	9.4
Accelerate	21	77.3	140	1.8	5.4
Mission I Totals			**14000**	**225**	**721**
Mission II					
Flight Phase	Qty.	Final Speed (ft/s)	Distance (ft)	Time (s)	Capacity (mAh)
Takeoff	1	32.0	37	1.8	8.99
Climb	1	51.4	410	8.7	40.3
First Leg	1	60.0	60	1.1	4.5
Cruise	2.66	77.3	1524	19.7	57.8
180 turn	6	60.6	-	2.4	8.1
360 turn	3	60.6	-	4.8	16.2
Accelerate	9	77.3	160	2.2	6.7
Mission II Totals			**6000**	**112**	**365**
Mission III					
Flight Phase	Qty.	Final Speed (ft/s)	Distance (ft)	Time (s)	Capacity (mAh)
Takeoff	1	32.0	37	1.8	8.99
Climb	1	51.4	410	8.7	40.3
First Leg	1	60.0	60	1.1	4.5
Cruise	2.66	77.3	1524	19.7	57.8
180 turn	6	60.6	-	2.4	8.1
360 turn	3	60.6	-	4.8	16.2
Accelerate	9	77.3	160	2.2	6.7
Mission III Totals			**6000**	**112**	**365**

Figure 5.7 – Mission Specific Performance

5.8 Drawing Package

In this section we present a full drawing package of the aircraft. The package includes a three view drawing, structural arrangements, the layout and location of various subsystems, and the accommodation of payloads for different missions.

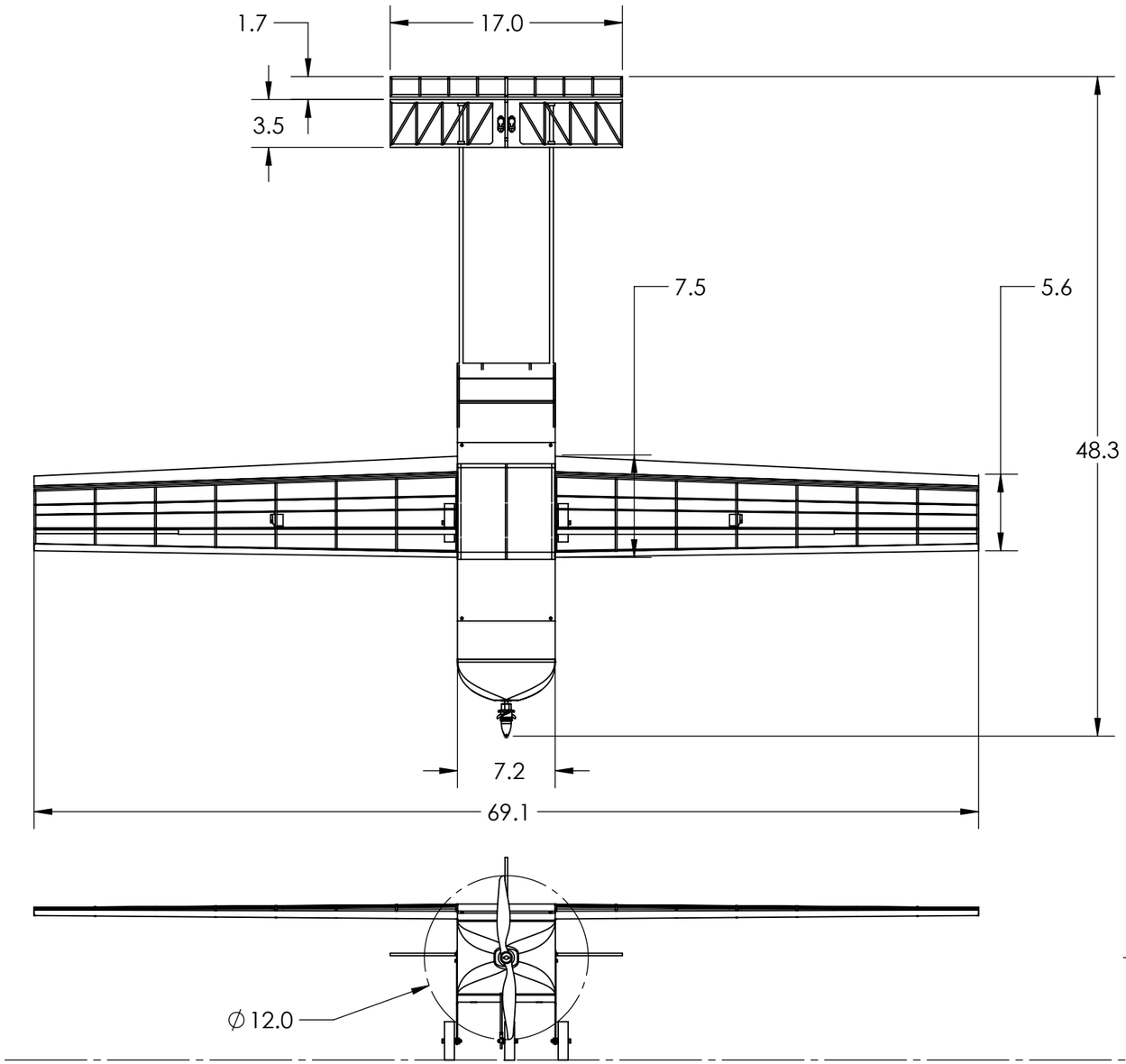

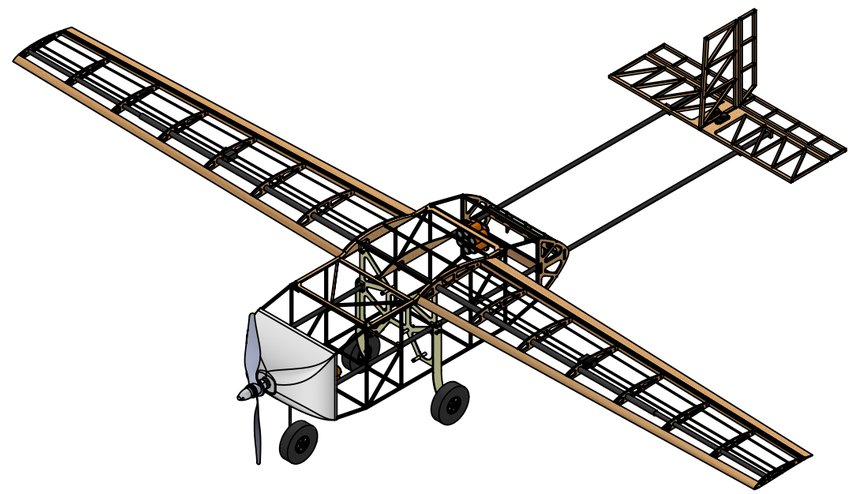

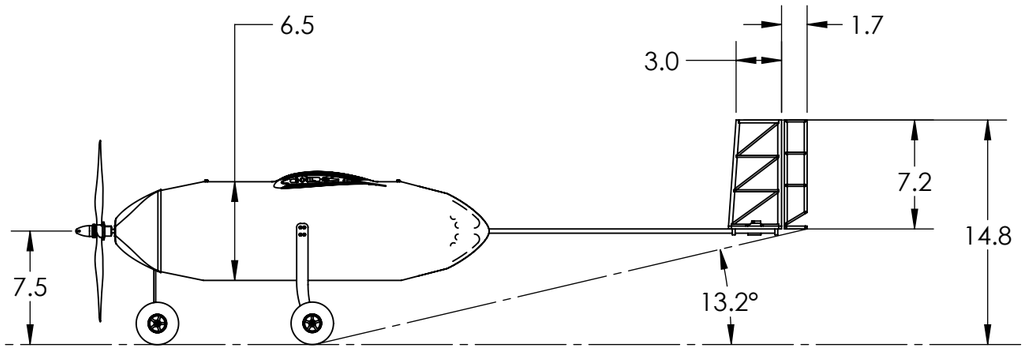

CORNELL UNIVERSITY DESIGN/BUILD/FLY 2014

TITLE

AIRCRAFT 3-VIEW

SIZE	SCALE	
B	1:4.5	DIMENSIONS ARE IN INCHES

	PART	MATERIAL	QTY
1	WING SPAR	CARBON FIBER	1
2	FUSELAGE SPAR	CARBON FIBER	2
3	WING	BALSA	1
4	TAIL	BALSA	1
5	WING BLOCK	POLYCARBONATE	2
6	TOP COVER	BALSA	1
7	BACK COVER	BALSA	1
8	FUSELAGE FRAME	BALSA	1
9	REAR BULKHEAD	SPRUCE	1
10	FRONT BULKHEAD	SPRUCE	1
11	MID BULKHEAD	FIBERGLASS	1
12	MAIN GEAR STRUT	FIBERGLASS	1
13	NOSE GEAR STRUT	CARBON FIBER	1
14	WHEEL	FOAM RUBBER	3
15	NOSE CONE	POLYSTYRENE	1

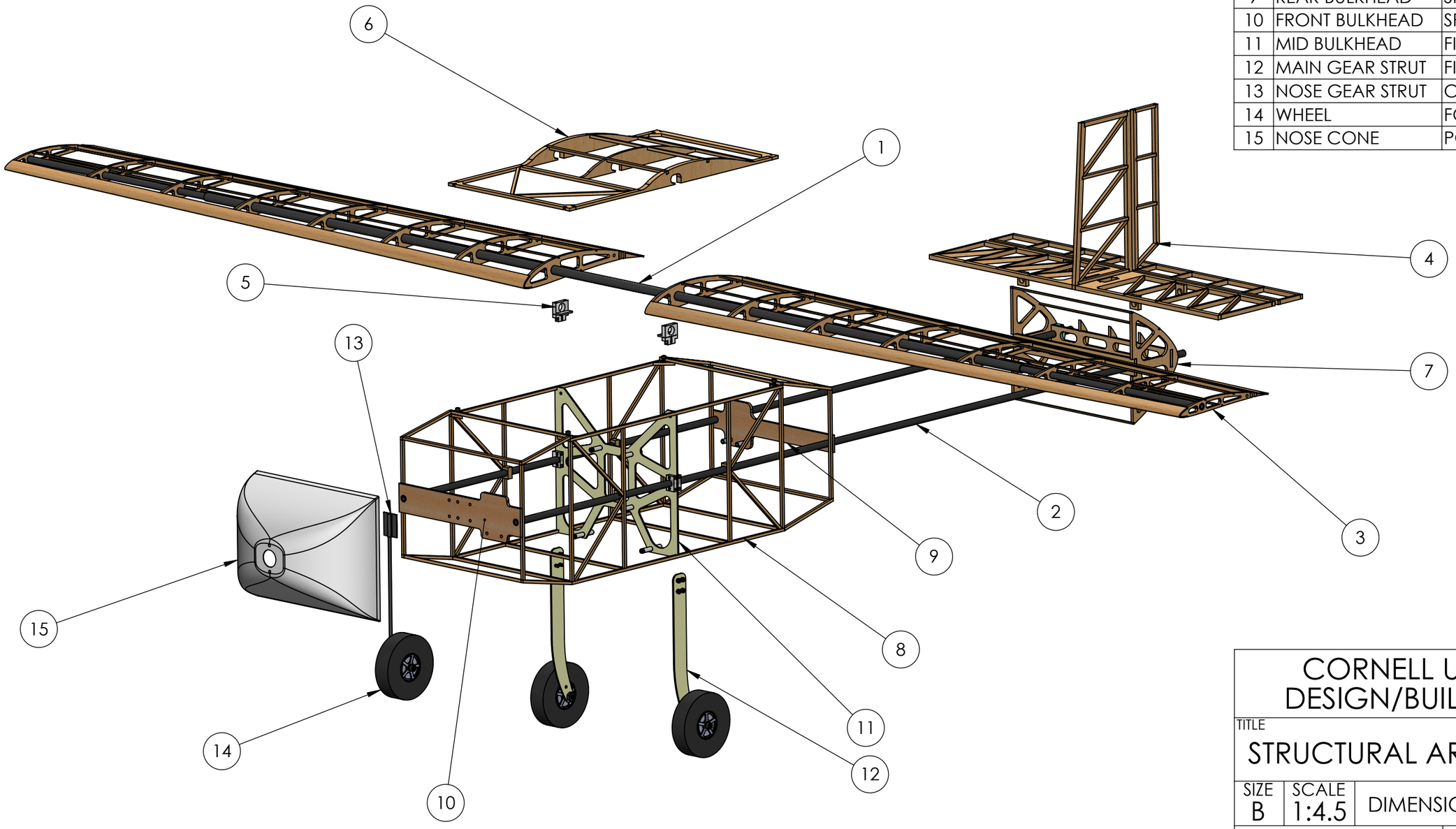

CORNELL UNIVERSITY
DESIGN/BUILD/FLY 2014

TITLE
STRUCTURAL ARRANGEMENT

SIZE	SCALE	
B	1:4.5	DIMENSIONS ARE IN INCHES

	PART	SOURCE	QTY
1	MOTOR	NEU 1105	1
2	GEARBOX	NEU P29	1
3	MOTOR BATTERY	ELITE 1500 mAh	14
4	RX BATTERY	KAN 125 mAh	4
5	SPEED CONTROLLER	TALON 25	1
6	RECEIVER	SPECTRUM AR6115e	1
7	SERVO	FUTABA S3114	4

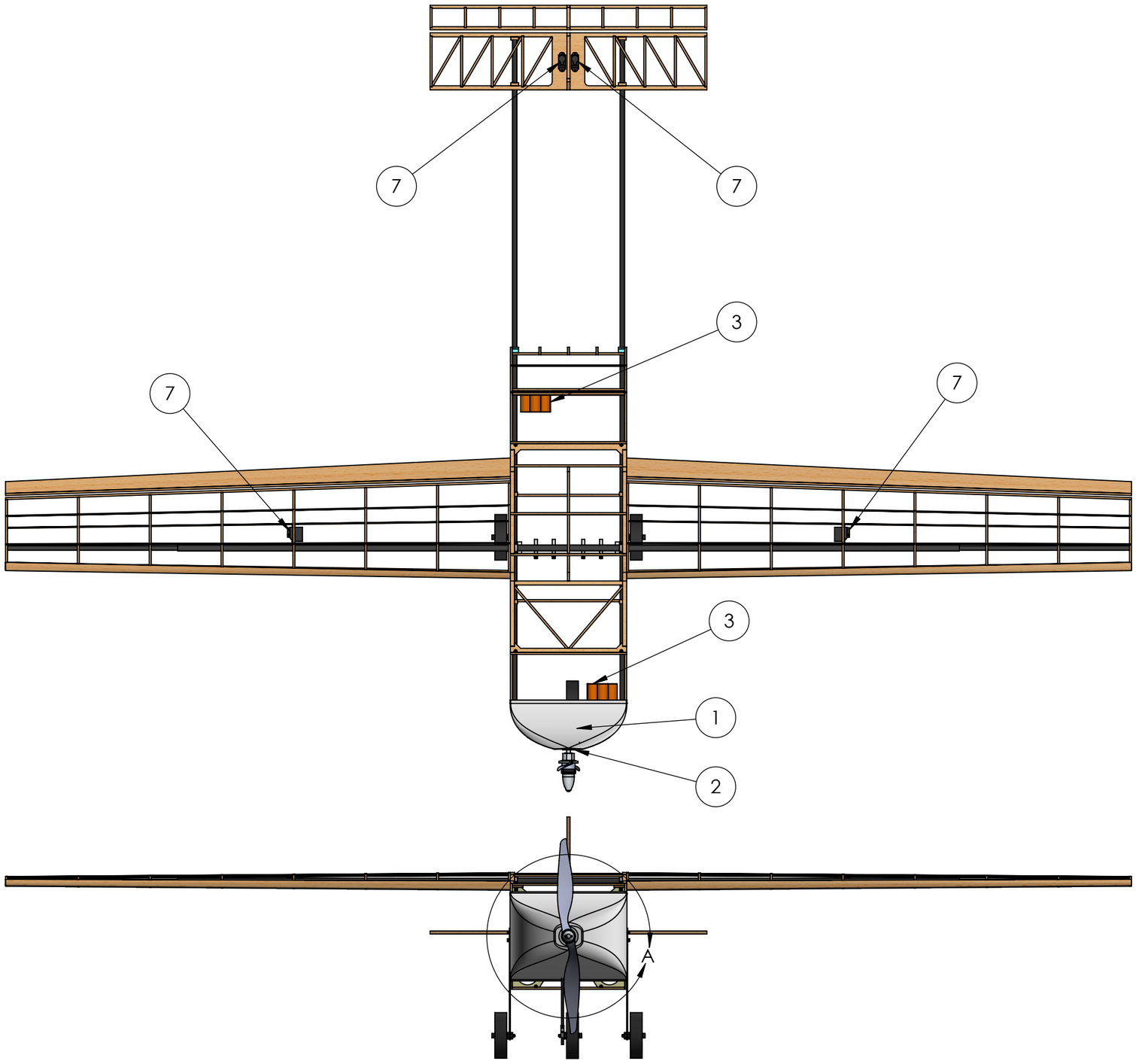

DETAIL A
SCALE 1 : 3

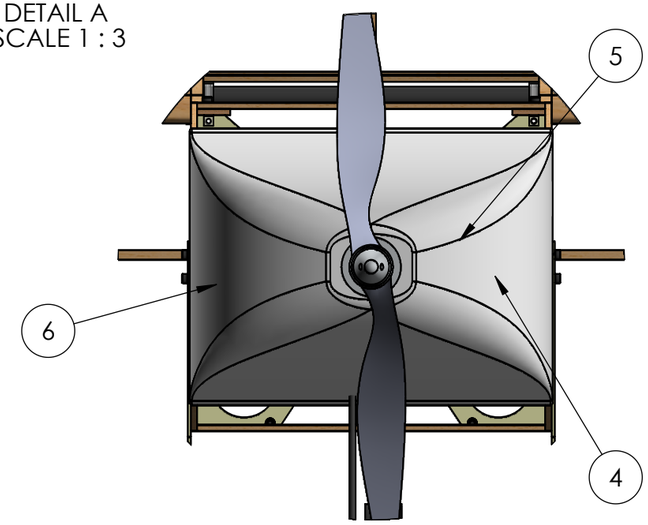

CORNELL UNIVERSITY
DESIGN/BUILD/FLY 2014

TITLE
SYSTEMS LAYOUT

SIZE	SCALE	
B	1:7	DIMENSIONS ARE IN INCHES

REPORT PAGE 43	SHEET 3 OF 4

MISSION 2 PAYLOAD ARRANGMENT

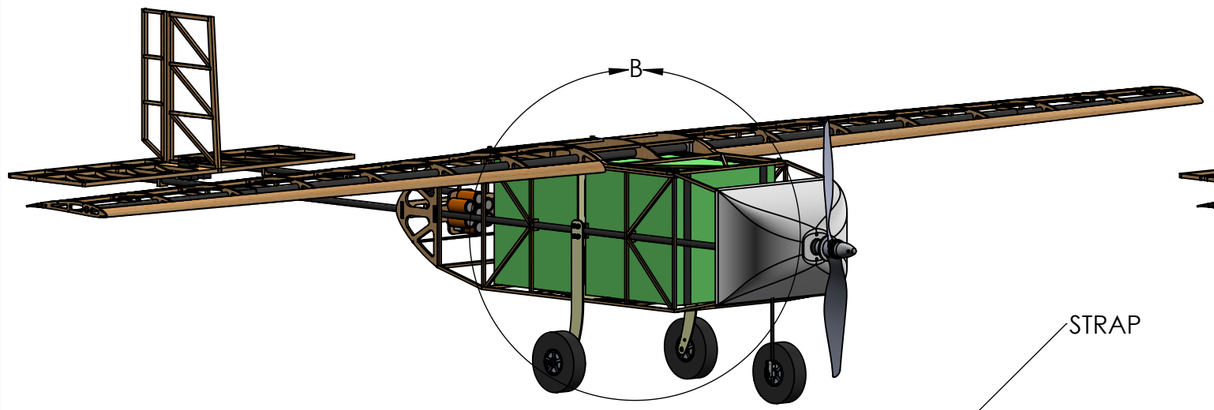

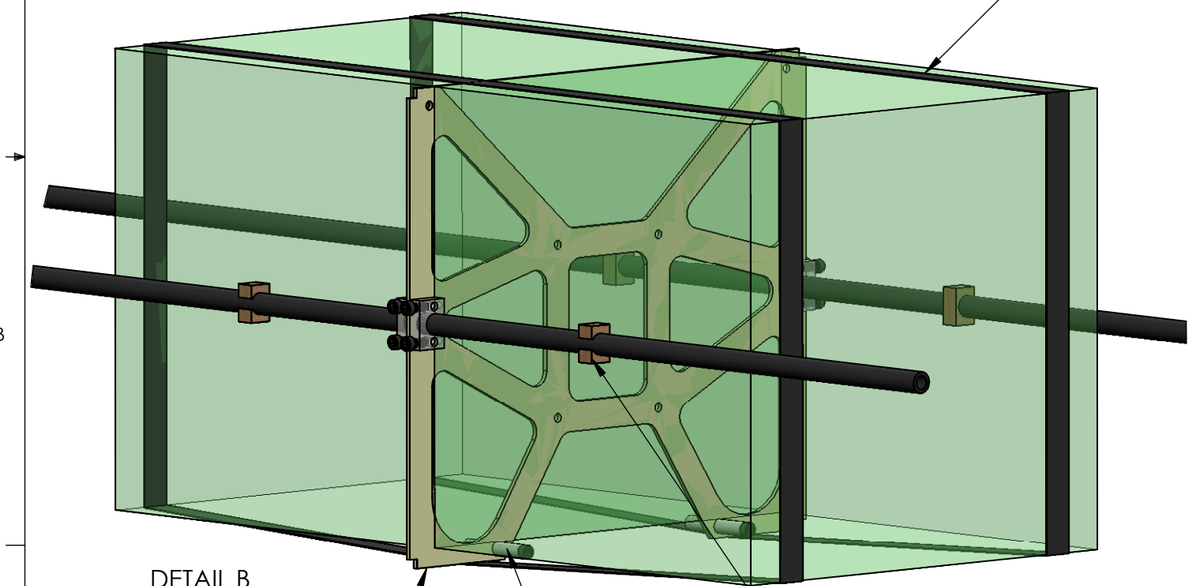

DETAIL B
SCALE 1 : 2

MISSION 3 PAYLOAD ARRANGMENT

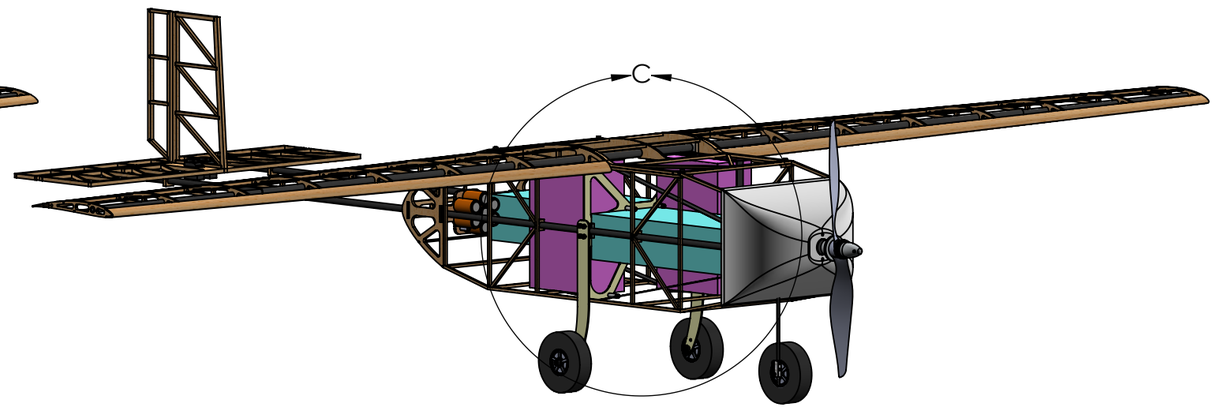

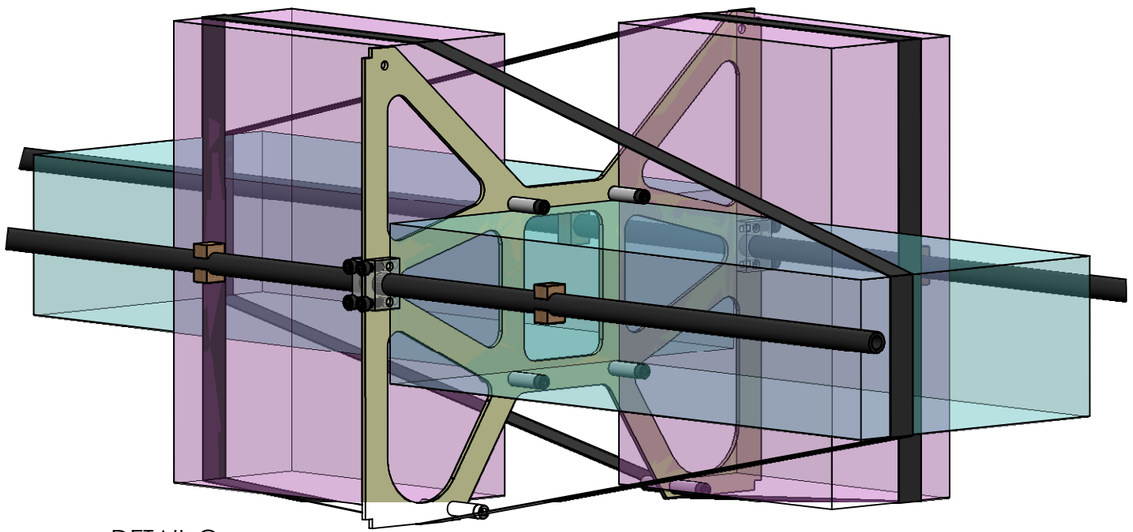

DETAIL C
SCALE 1 : 2

CORNELL UNIVERSITY
DESIGN/BUILD/FLY 2014

TITLE
PAYLOAD ACCOMODATION

SIZE	SCALE	
B	1:7	DIMENSIONS ARE IN INCHES

REPORT PAGE 44	SHEET 4 OF 4

6 Manufacturing Plan and Processes

As a part of the design process, the team determined optimal processes for manufacturing the aircraft's major components. Upon completion of the design, we created a timeline for aircraft construction that would ensure that we meet our flight testing milestones. The plan, shown in figure 6.0, enables us to complete three successive iterations on our design, with time allotted between iterations for optimization work.

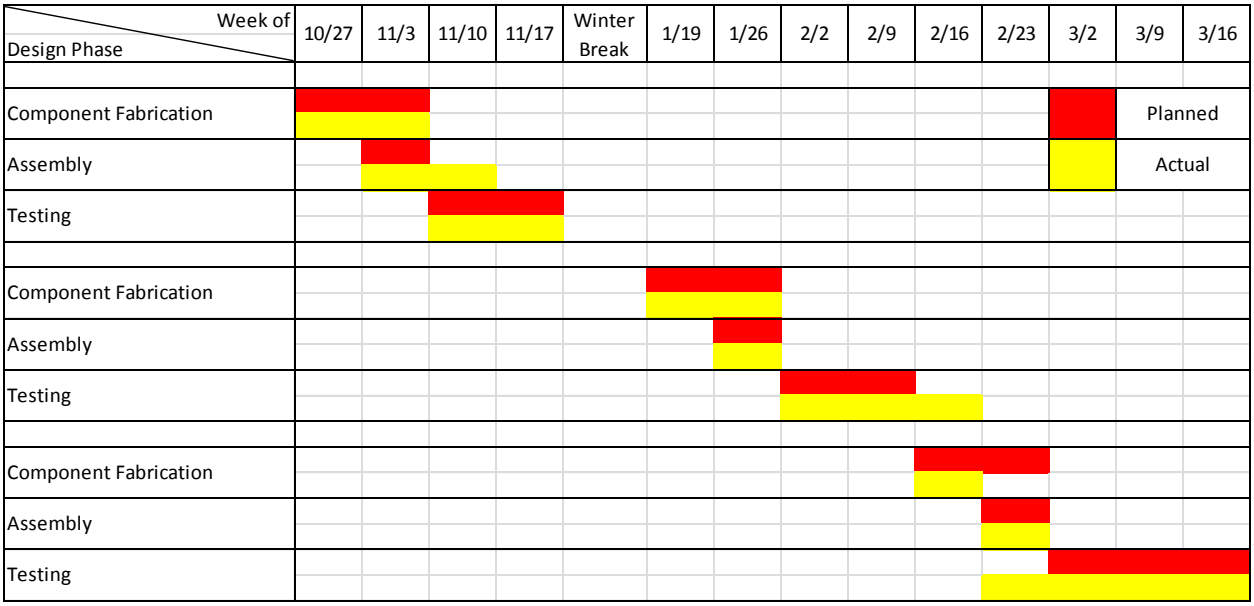

Figure 6.0 – Manufacturing schedule

6.1 Manufacturing Process Selection

Manufacturing and construction methods play a crucial role in the weight and strength of an aircraft design. Our team considered three major fabrication methods for our design, with the following characteristics:

- **Balsa Build-up –** With exceptional strength to weight ratio, this method provides great scoring characteristics and a modest amount of manufacturing complexity.
- **Foam –** This method provides a fast manufacture process but also usually results in heavier components than a comparable balsa build-up.
- **Carbon Fiber –** This method yields extremely strong components that are often heavier than either balsa or foam. It provides flexibility to create nearly any shape that is desired, or can be purchased in a number of preformed shapes.

We compared these methods based on aircraft weight, strength, and manufacturability in figure 6.1. Our decision to manufacture the majority of the aircraft using a balsa build-up can be attributed to aircraft weight's large impact on the scoring. In areas of significant structural loading, the aircraft utilizes a small

number of carbon fiber components for added strength. The remainder of the craft is constructed of custom laser cut balsa and spruce components.

Category	Weight	Balsa Build-up	Foam	Carbon Fiber
Weight	0.5	4	3	3
Strength	0.3	4	3	5
Manufacturability	0.2	3	3	2
Total	**1**	**3.8**	**3**	**3.4**

Figure 6.1 – Manufacturing process selection

6.2 Subsystem Manufacturing

This section describes the fabrication of the major subsystems of the aircraft including: wing, fuselage, empennage, nose cone, and propulsion subsystems.

6.2.1 Wing manufacturing

The wing is composed of laser cut balsa ribs, one main telescoping spar, stringers, and mounting blocks. We aligned the wing components using the main spar, an auxiliary spar, and wooden jigs that support the spars at the tips. We aligned the ribs span-wise using a printed drawing plan. Epoxy was used to glue all carbon fiber joints and CA glue for noncritical wood joints. Wetted balsa sheets were folded over the leading edge of the ribs to form the wing's leading edge. Stringers and leading edge balsa sheeting provided attachment surfaces for Mylar covering.

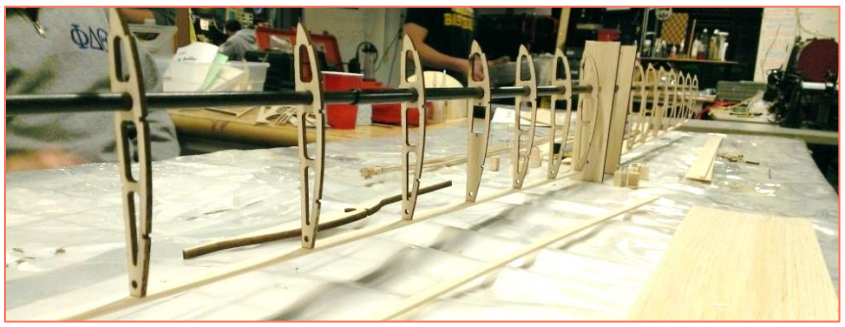

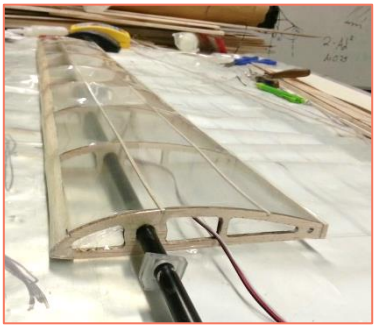

Figure 6.2.1 – Wing Manufacturing

6.2.2 Fuselage manufacturing

Fuselage manufacturing began by assembling the balsa side panels with the aid of a layout diagram. These panels were then stood upright and connected to each other via balsa crossmembers and structural bulkheads made of laser cut G10 garolite or spruce. The longitudinal booms were passed through the structure prior to gluing to ensure proper alignment. Structural joints were made using two part epoxy and non-structural joints with CA glue. The rear fuselage cap was assembled separately and

slid onto the tail booms. The hatch door was also assembled separately with the use of a layout diagram. Finally, the entire fuselage was coated with mylar film to create it's aerodynamic shape.

Figure 6.2.2 – Fuselage manufactuing

6.2.3 Empennage manufacturing

The horizontal and vertical stabilizers, as well as elevator and rudder, were constructed with a series of laser cut balsa parts. Each section was assembled flat on a foamboard with the help of a layout diagram. Once formed, each of the panels was coated with mylar to form the aerodynamic surface. The vertical stabilizer was then glued into slots in the horizontal stabalizer and control surfaces were attached using CA hinges. Once complete, the entire tail assembly was mounted on the tail booms using a series of balsa wood attachment brackets.

Figure 6.2.3 – Empennage manufacturing

6.2.4 Nosecone manufacturing

The nosecone was constructed by using a process called vacuum-forming. A hard-foam mold of the nosecone profile was cut by a router. A sheet of polystyrene was stapled to a wooden frame and heated in an oven to 450 degrees Fahrenheit. After several layers of mold release were applied to the foam, it was placed on a vacuum table. The hot sheet was then placed over the mold and the vacuum extracted the air between the mold and the plastic, hardening the plastic into the shape of the nosecone.

Figure 6.2.4 – Nosecone Manufacturing

6.2.5 Landing gear manufacturing

In order to attach the 1/8 inch carbon fiber rod to the front bulkhead, two layers of carbon fiber weave were added to one end of the rod. The first step was to take a piece of glass, and wax it with mold release. After several coats, a square of the weave was placed on the glass and covered in epoxy. The rod was then laid down along the center axis of the square, and covered with another epoxy-soaked square weave. The assembly was then covered with perforated release film, peel ply, breather, and a vacuum bag sealed with gum tape. With a vacuum attached, it was left to cure overnight.

Figure 6.2.5 – Landing gear manufacturing

6.2.6 Propulsion manufacturing

The majority of the propulsion system components were commercially purchased as is mandated by the competition rules. The motor mounting plate was laser cut from a sheet of g10 garolite. The other main task of propulsion system manufacturing was the assembly of battery packs. We assembled each

battery pack from loose cells. We formed connections using solder braid in order to ensure low resistance and weight. Lightweight Kapton tape provides electrical insulation for the packs.

Figure 6.2.6 – Propulsion manufacturing

7 Testing Plan

This section of the report details the team's plans for testing of subsystems and our complete aircraft design. The purpose of these tests is to validate our performance estimates and to identify areas of the design that need improvement or show potential for increasing competition score. Figure 7a shows a checklist of our major testing objectives.

Structural Testing
☑ *Wing loading*: The wing must be able to sustain loading conditions that will be experienced during flight maneuvers. A wing tip load test simulates the worst case loading condition.
Payloads Testing
☑ *Attachment strength*: The payload attachment system must be strong and secure enough to prevent any movement of the payloads during flight, namely during taxiing and landing.
Propulsion Testing
☑ *Static Thrust Testing*: Thrust and current draw must be verified against theoretical calculations at the static condition to ensure that the take-off distance and current limitations are met.
Complete Aircraft Testing
☑ *Taxi Testing*: The craft must be robust and provide adequate control in navigating the taxi mission terrain. ☑ *Take-off distance*: We must take off within a forty foot long runway when fully loaded. ☑ *Trim*: The aircraft must demonstrate adequate trim in both takeoff and cruise conditions. ☑ *Directional/roll/pitch control*: Control surface sizing will be verified by observation of acceptable roll, bank, and climb rates. ☑ *Stall recovery*: The aircraft must recover from a stall with minimum altitude loss. ☑ *Mission Performance*: Each mission will be completed to verify predictions of mission performance

Figure 7a – Testing checklist

Figure 7b shows the team's timeline of planned and executed testing. Weather conditions have adversely affected our test schedule, but extra time built into the schedule will allow us to recover from this setback.

Testing \ Week of	11/10	11/17		2/2	2/9		2/16	2/23	3/2	3/9	3/16
	Aircraft 1			Aircraft 2			Aircraft 3				
Structural										Planned	
Propulsion										Actual	
Payloads											
Taxi Mission											
Empty Flight											
Mission One											
Mission Two											
Mission Three											

Figure 7b – Testing schedule

7.1 Propulsion Testing

The propulsion subteam completed a series of tests on propulsion components in order to confirm theoretical predictions, as well as optimize propeller selection and battery size. As a consideration of the takeoff distance constraint, the team also examined the effects of throttle advance rate on current draw. We developed a fixture to measure thrust that employed a 25-lb, S-band load cell (Figure 7.1). During thrust testing, we used a Castle Creations speed controller to log data of electrical parameters.

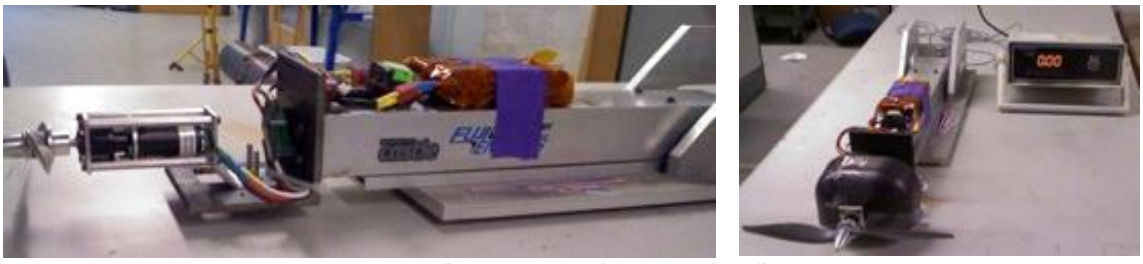

Figure 7.1 – Thrust testing fixture

7.2 Structural Testing

The main focus of structural testing was the structural integrity of the main wing spar. A wingtip-loading test was done in order to simulate a 5g turn and ensure that the spar could withstand those forces. Through stress analysis, we determined that a 2g wing tip test would simulate the desired 5g turn.

Using a prototype wing, we secured the wing tips to two tables such that the majority of the wing was hanging freely between the two tables. We then placed a box at the wing root, and placed weights in the box until we reached the 2g we desired. Along the way we recorded multiple steps of adding weight and the amount that the wing displaced.

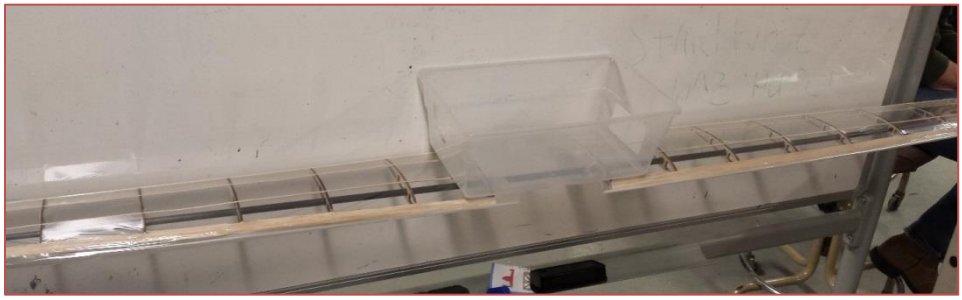

Figure 7.2 – Wing structural testing.

7.3 Payloads Testing

The method for securing the payloads was extremely important throughout design. In order to ensure proper stability of the aircraft, it is vital that each missions' payloads are properly secured. To test methods of payload attachment, a prototype fuselage was created, along with a few different methods for securing the payloads. Straps, Velcro straps, pins, and a structural fuselage were all tested throughout our design process. Each attachment method was tested to make sure the payloads were completely constrained.

7.4 Full System Testing

Full system testing provides us with the most comprehensive account of design validation. Through a progress of envelope expansion, we are able to validate all of our performance characteristics while reducing the risk associated with such tests. Our testing progresses from validating basic handling characteristics to simulating competition flights through a number of steps, shown in Table 7.4. This series of tests is to be conducted for each aircraft that is constructed. Flight testing covers a large portion of time to account for unforseen delays.

Test #	Testing description/goals
1	Taxi test: Ensure ground control and aircraft robustness.
2	Maiden flight: Set empty aircraft trim, observe handling characteristics.
3	Fly rectangular patterns and figure eights; test stall and spin recovery.
4	Fly mission one; record flight time and current draw.
5	Fly mission two; record flight time and current draw.
6	Fly mission three; record flight time and current draw.

Table 7.4 – Flight testing plan for each aircraft

8 Performance Results

This section outlines the performance results measured and recorded during subsystem and complete aircraft testing. We use the results of these tests to validate performance estimates and optimize the aircraft design. Any discrepancies or unexpected problems are analyzed and used in the design of the next aircraft iteration.

8.1 Propulsion Results

Figure 8.1a shows a sample of the data collected for propulsion thrust testing using the Castle Creations speed controller. The output displays motor RPM, voltage, and current draw versus time for a range of motor-propeller combinations.

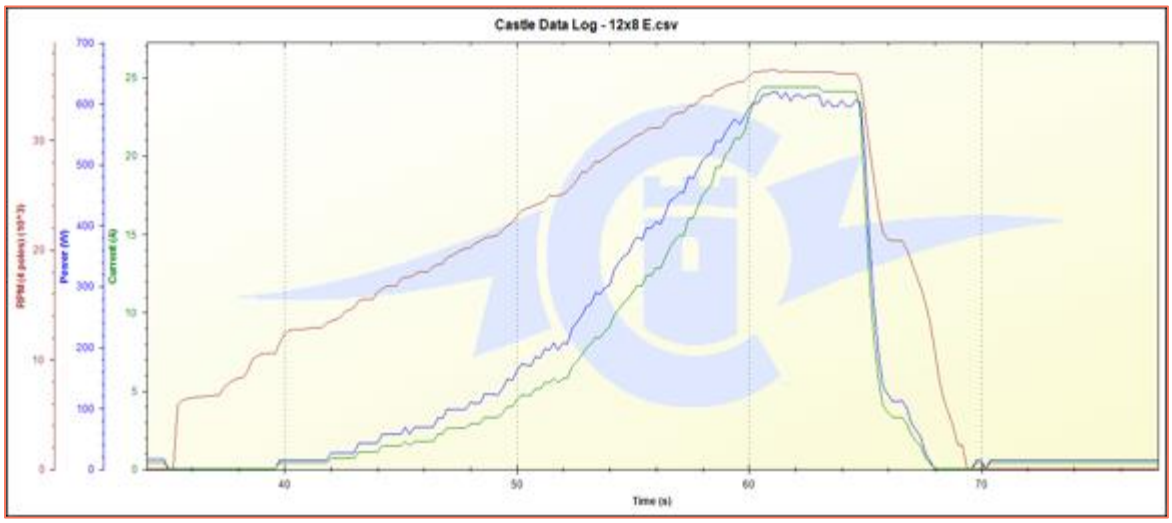

Figure 8.1a – Sample of data collected for propulsion thrust testing

These results agreed relatively well with our expected values. From this series of tests, we concluded that we could use a larger than expected propeller and operate above the listed current limit without blowing the fuse. These results will lead to further testing to determine a more accurate value of current limit.

Propeller	Thrust (lbf)	Current (A)	Power (lbs*ft/s)	Motor RPM
12x10 E	2.9	13.9	186	37500
13 x 8 E	3.4	15.2	196	36300
14 x 8.5 E	3.7	17.4	213	35900

Figure 8.1b – Static propulsion performance

8.2 Structural Results

The values recorded during the wingtip-loading test are plotted in the figure below. The deflection of the wing root was approximately linear with the load placed on the root. The wing successfully withstood the loading equivalent of a 5g turn, and showed elastic behavior throughout testing. Our measured values agree very closely with the results that were predicted from the structural model. Any slight differences between the predicted and actual structure can be attributed to the assumption that the load was distributed across the entire spar.

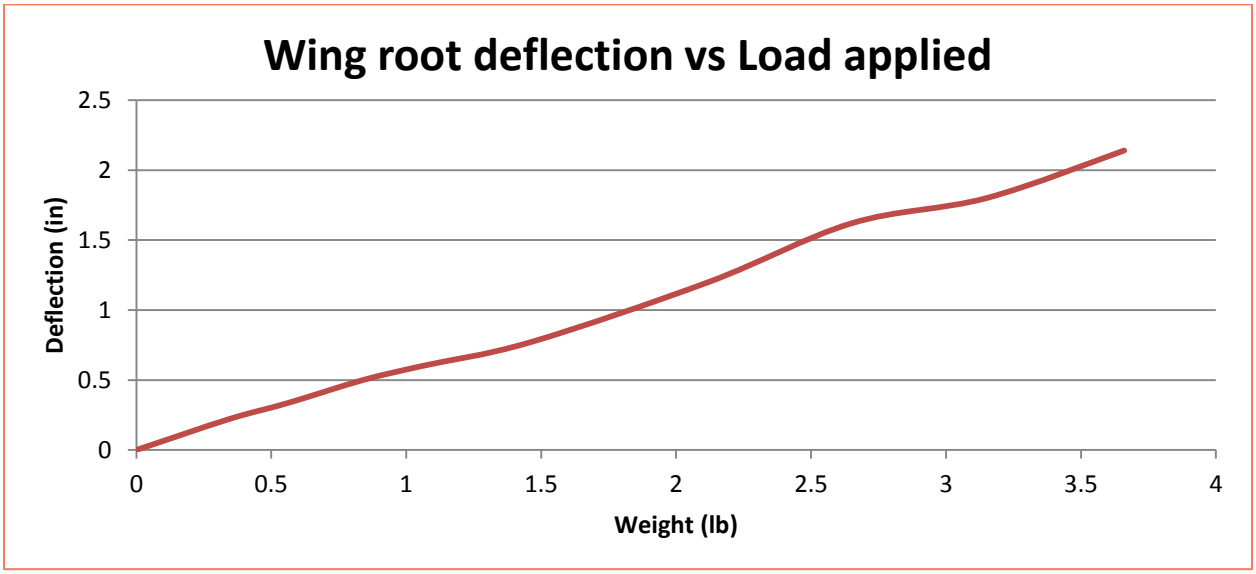

Figure 8.2 – Wingtip testing results

8.3 Payloads Results

After testing each payload attachment method, it was determined that a simple system of straps and pins would be the optimal method for securing the payloads. In addition to facilitating rapid and secure attachment, this system is also extremely lightweight. One additional outcome of this testing was to increase the size of the hatch opening. This provides the user with more handling clearance and prevents damage to the fuselage during payload installation.

Figure 8.3 – Constrained payloads

8.4 Full System Results

This section details the results of tests performed on our complete aircraft solution, including taxi testing and aircraft handling. These tests were completed across iterations one and two of our design, and will continue after the submission of this report.

8.4.1 Taxi testing

Taxi testing was completed by building a course representative of that which will be used at competition. Several attempts were made to traverse the course with gradually increasing success. We discovered that increased speed improved the ability to adequately control the craft. Additionally, large foam wheels were the best option for decreasing the shock experienced by the aircraft during the test. This test was helpful in validating our ability to navigate the course without damage. The team will continue to test on this course in order to determine an optimal plan for effective navigation that avoids damage to the aircraft.

Figure 8.4.1 – Rough Field Taxi testing

8.4.2 Flight testing

Unfortunately our flight testing schedule has been adversely affected by weather conditions. A particularly harsh Ithaca, NY winter has prevented us access to a safe and suitable location to conduct flight testing on our second design iteration. Therefore, flight testing has been limited to our first prototype. Additionally, our first aircraft did not survive its maiden flight. The flight began well, with the aircraft taking off within 20 feet and flying controllably for approximately the 15 seconds. However, after this period, the aircraft developed a quickly and consistently worsening left roll. After another minute of efforts to regain control, the prototype crashed, suffering irreparable damage. Figure 8.4.2a shows this prototype in flight. Our analysis of the crash resulted in the list of likely causes shown in figure 8.4.2b.

Figure 8.4.2a – Aircraft #1 flight testing.

Potential Cause	Description	Proposed correction
Wing Twist	A broken glue joint could cause one wing to rotate relative to the other about the spar	Change to one piece wing design
Weak Flaperons	Flaperons could have flexed non-uniformly	Strengthen flaperons
Wing Deflection	Two piece wing design also caused larger than expected wing deflection under load.	Change to one piece wing design

Figure 8.4.2b – Potential crash causes and plans for correction

We are confident that after making these changes, our second design iteration will perform far better. Our team is anxiously awaiting acceptable flying conditions and we anticipate rapid progression through our test plan during the week following submission of this report.

9 References

"2012/2013 Rules and Vehicle Design." *AIAA DBF*. Web. 31 Aug. 2013. http://www.aiaadbf.org/2013_files/2013_rules.htm

"Airfoil Database Search." *Airfoil Tools*. Web. Sep. 2013. http://airfoiltools.com/search/index

Anderson, John. Introduction to Flight. 6th. New York: McGraw-Hill, 2005.

Caughey, David A. *Introduction to Aircraft Stability and Control Course Notes for MAE 5070*. Ithaca, NY: Cornell University, 2011. *MAE 5070 Dynamics of Flight Vehicles*. 12 Apr. 2011. Web. 27 Sept. 2013. <https://courses.cit.cornell.edu/mae5070/Caughey_2011_04.pdf>.

Drela, M., & Youngren, H. XFOIL. Retrieved Sep. 2013, from Subsonic Airfoil Development System: http://web.mit.edu/drela/Public/web/xfoil/.

Drela, M., & Youngren, H. AVL. Retrieved Jan. 2014, from http://web.mit.edu/drela/Public/web/avl/.

Etkin, B., & Reid, L. D. Dynamics of Flight Stability and Control Third Ed. Hoboken, New Jersey: John Wiley and Sons, 1996

Gilruth, R. R., and M. D. White. "Analysis and Prediction of Longitudinal Stability of Airplanes." *NASA Technical Reports* 711th ser. 1941.

Krauss, Tom. Airfoil Investigation Database. November, 2013. http://www.worldofkrauss.com

Muller, Markϋs. “propCalc – Calculator for Propeller, Powered by Neu Motors”. *Neu Motors*. Web. Oct. 2012. http://www.ecalc.ch/motorcalc_e.asp?neumotors

Nelson, Robert C. Flight Stability and Automatic Control. 2nd ed. Boston, MA: WCB/McGraw Hill, 1998. Print.

Raymer, Daniel. Aircraft Design: A Conceptual Approach. 3rd. Washington, D.C.: American Institute of Aeronautics and Astronautics, Inc., 1999.

Shevell, R. S., Fundamentals of Flight, 2th Prentice Hall, 1989.

UIUC Airfoil Coordinate Database. Web. Nov. 2013. http://www.ae.uiuc.edu/mselig/ads/coord_database.html